RIVISTA DEL NUOVO CIMENTO VOL. 24, N. 7 2001

Dynamic nonlinear elasticity in geomaterials

L. A. OSTROVSKY[1][2] and P. A. JOHNSON[3]

([1]) *University of Colorado, CIRES/NOAA Environmental Technology Laboratory Boulder, CO, USA*

([2]) *Institute of Applied Physics, Russian Academy of Science 46 Ul'yanov St. 603600 Nizhny Novgorod, Russia*

([3]) *Los Alamos National Laboratory - Los Alamos, NM, USA*

(ricevuto il 13 Novembre 2000)

2 1. Introduction and background
2 1·1. On "classical" nonlinear acoustics
4 1·2. Nonlinearity and earth materials
5 2. Key experimental indicators of nonlinearity in rocks
5 2·1. Quasi-static experiments
7 2·2. Dynamic indicators
7 2·3. Nonlinear resonance frequency shift
10 2·4. The effect of fluids
10 2·5. Slow dynamics
11 2·6. Harmonic generation
12 2·7. Wave modulation experiments
12 2·8. Nonlinear dissipation
17 2·9. Experiments with travelling waves
19 2·10. Noncollinear interactions of acoustic beams
20 3. Theoretical models
21 3·1. Classical theory
22 3·2. Phenomenological models with hysteresis
24 4. Physical models of structural nonlinearity
26 4·1. Hertzian contacts
28 4·2. "Bed of nails" model of cracks
29 4·3. The role of fluids in the bond system
31 4·4. The role of transverse deformations
31 4·5. Granato-Lücke model
32 4·6. Slow dynamics
33 5. Nonlinear waves in rocks
33 5·1. Travelling waves
34 5·2. Travelling waves and hysteresis
35 5·3. Standing waves in resonators
37 5·4. Numerical simulations
39 6. Field experiments
39 6·1. Active observations
39 6·2. Earth tides and nonlinear response
40 6·3. Strong ground motion
40 7. Potential applications
40 7·1. Nondestructive testing of materials
43 8. Conclusions

1. – Introduction and background

The nonlinear elastic behaviour of earth materials is an extremely rich topic, one that has broad implications to earth and materials sciences, including strong ground motion, rock physics, nondestructive evaluation and materials science (*e.g.*, [1, 2]). The mechanical properties of rock appear to place it in a broader class of materials, one we call the *Structural Nonlinear Elasticity* class (also *Mesoscopic/Nanoscale Elasticity, or MS/NSE class*). These terms are in contrast to materials that display classical, *Atomic Elasticity*, such as most fluids and monocrystalline solids. The difference between these two categories of materials is both in intensity and origin of their nonlinear response. The nonlinearity of atomic elastic materials is due to the atomic/molecular lattice anharmonicity. The latter is relatively small because the intermolecular forces are extremely strong. In contrast, the materials considered below contain small soft features that we term the "bond system" (cracks, grain contacts, dislocations, etc.) within a hard matrix (grains, crystals), producing very large nonlinear response. In these materials, hysteresis and relaxation (slow dynamical effects) are characteristic, none of which appear in atomic elastic materials.

We begin with a brief historical background from nonlinear acoustics to the recent developments in rock nonlinearity. This is followed by an overview of some representative laboratory measurements which serve as primary indicators of nonlinear behaviour, followed by theoretical development, and finally, mention a variety of observations of nonlinearity under field conditions and applications to nondestructive testing of materials.

Our goal is not to survey all papers published in the area but to demonstrate some experimental and theoretical results and ideas that will help a reader to become oriented in this broad and rapidly growing area bridging macro-, meso-and microscale (nanoscale) phenomena in physics, materials science, and geophysics.

1·1. *On "classical" nonlinear acoustics.* – The term "nonlinear acoustics" refers to acoustical waves in compressible media that have small but finite amplitudes. These waves are described by nonlinear equations following from the general governing equations of continuous media for moderate-amplitude displacements when the nonlinear terms are small compared with the linear ones (which does not mean that their effect on the process is small!). For fluids, the fundamental achievements in the theory of nonlinear waves were made in 18th and 19th centuries by Euler, Lagrange, Poisson, Stokes, Riemann, Rankine, Hugoniot, and others. In particular, a cumulative steepening of a nonlinear wave with its eventual "breaking" and formation of a discontinuity-shock wave (fig. 1) was predicted after intensive research and discussions. Specific problems related to the development of nonlinear acoustics were then considered by Rayleigh, Eikhenwald, and later, in the 1930s, by Fay and Fubini who proposed solutions describing harmonic generation in sound waves. In 1935 Thuras and Jenkins were apparently the first to investigate this phenomenon experimentally. An important step was made in 1948 by Eckart who derived solutions to nonplanar finite-amplitude sound waves.

It was not until the late 1940s and into the early 1960s, however, that the domain of nonlinear acoustics began to develop into an organized discipline. This was due originally to the development of jet aircraft at the end of world war II, and to naval applications, especially to the development of the *parametric array* by Westervelt in the USA and Zverev and Kalachev in Russia, in the late 1950s-early 1960s. The idea behind the parametric array is to obtain directed radiation of a low-frequency signal from the nonlinear

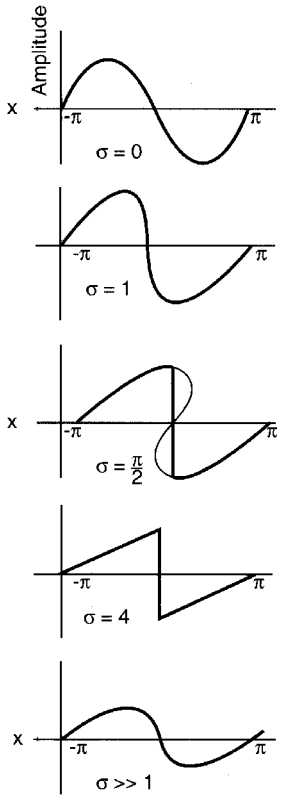

Fig. 1. – Wave distortion as a function of normed distance, σ ($\sigma = 1$ corresponds to the beginning of shock formation). The bottom figure is for large distances ($\sigma \gg 1$) when the wave returns to an almost harmonic profile due to stronger damping of higher harmonics.

interference of two narrow, finite-amplitude, overlapping high-frequency acoustic beams close in frequency to each other. Nonlinear interaction between the two beams creates a difference-frequency wave generated throughout the volume of interaction (fig. 2). Such a system can be used as a "virtual" antenna that radiates a directed, low-frequency signal without sidelobes. The idea can be applied in reverse, as well, to the reception of a small low-frequency signal by interaction with a strong high-frequency acoustic beam. Despite their low efficiency, parametric arrays have found their application, particularly in marine sonars (see, *e.g.*, [3]).

The experiments on dynamic nonlinear effects in *solids* started as early as in 1950s. Detailed experiments on harmonic generation in crystals were performed by Zarembo and Krasil'nikov in Russia and, most thoroughly, by Breazeale in the USA; for early results see, *e.g.*, [4]. Anomalously strong hysteretic nonlinearities in metals were observed that probably correspond to the structural (mesoscopic) nonlinearity associated with dislo-

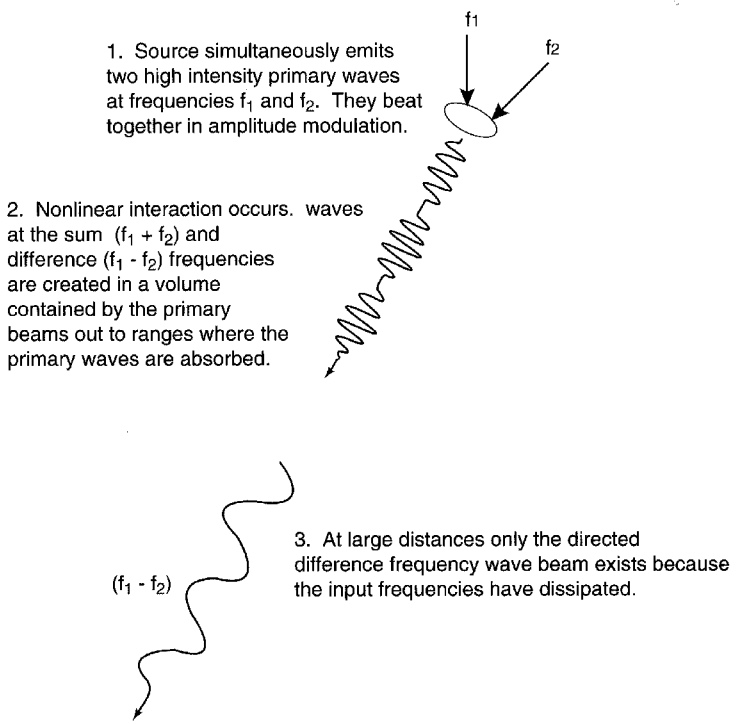

Fig. 2. – Concept of the parametric array.

cations (*e.g.*, [5]). In an acoustical experiment with a metal ring resonator [6] effects of strong dynamic nonlinearity([1]) were observed which included harmonic and subharmonic (parametric) generation and slow relaxation of nonlinearity (slow dynamics) which are presumably due to mechanisms of structural nonlinearity discussed below for rocks.

More recently, various other applications of nonlinear acoustic effects in nondestructive material testing, biology, and other areas have been developed to some degree, and these areas are also growing rapidly. New physical effects such as self-focusing, wave front reversal, and others similar to those seen in laser optics and plasma physics have been observed. For more information on nonlinear acoustics see the recent book by Naugolnykh and Ostrovsky [7] and the paper collection edited by Blackstock and Hamilton [8].

1·2. *Nonlinearity and earth materials.* – In the 1940s Birch's group at Harvard University began study of the static nonlinear properties of rock [9]. These studies, conducted in large mechanical presses, were designed to interrogate the stress-strain relation (or the equation of state, EOS, as we will call it here) in rock samples at strong, low-frequency

([1]) Here *dynamic elastic nonlinearity* is defined specifically to include wave studies in materials at dynamic strains approximately equal to and less than roughly 10^{-4}.

forcing (near dc). Static tests were aimed at interrogating the nature of the earth's interior in terms of pressure and temperature response, and to predict mineral assemblages and mineral phases in the earth's lower crust and mantle. These studies have been invaluable in understanding and modeling physical properties and inferring the composition of the earth's interior.

In the late 1950s and early 1960s, shock wave physical experiments aimed at obtaining high pressure-temperature dynamic elastic constants of minerals were undertaken. Much of the early work in this area was developed in Los Alamos (USA) by McQueen and his colleagues, for instance.

In the early 1970s, Stacy's group at the University of Queensland wrote a series of papers on mechanical hysteresis in rocks at low strains [10]. Their work showed that nonlinear response persists in quasistatic tests at strains as low as 10^{-6}, and perhaps lower. Some of the first low-strain nonlinear elasticity studies (strains of the order of 10^{-7}) of which we are aware dealed with nonlinear effects so that they could be avoided in linear, resonant bar wave studies [11].

In the early 1980s Bakulin and Protosenya [12] and a group at the Radiophysical Institute and the Institute of Applied Physics in Nizhny Novgorod, Russia began studies of nonlinear response in earth materials. In parallel, the idea of the parametric array as applied to the earth led researchers in Los Alamos into dynamic nonlinear elasticity studies beginning in 1982.

As early as 1986, there was an international symposium on nonlinear seismology organized by the Moscow Earth Physics Institute, held in Sudzal, USSR, and soon thereafter, a special issue of *Physics of the Earth and Planetary Interiors* (vol. **50**, No. 1, 1987) devoted to nonlinear seismology appeared. More recently, in 1996-1999, the first four International Workshops on Nonlinear Mesoscopic Elasticity were held at the Institute of Geophysics and Planetary Physics at Los Alamos National Laboratory, the fifth was held in 2000 in Santa Margarita Ligure, Italy, and the sixth in Leuven, Belgium, at the Catholic University.

2. – Key experimental indicators of nonlinearity in rocks

Dynamic nonlinear response may manifest itself in a variety of ways, including resonant frequency shift, harmonic generation, frequency mixing, nonlinear attenuation and slow dynamical effects, all of which will be illustrated below. Here we present some key indicators of nonlinear behaviour from static and, mostly, dynamic data from laboratory experiments. These experiments provide not only qualitative but also quantitative measures of the nonlinearity.

2·1. *Quasi-static experiments.* – The most fundamental observation of elastic nonlinearity in solids comes from quasi-static tests of stress *vs.* strain. Figure 3a shows a typical experimental configuration where stress is induced along the axis of a sample, and strain was measured in the same direction. Figure 3b shows a pressure history "protocol" for one such experiment and fig. 3c shows experimental results illustrating such a dependence (*e.g.*, [13-15]). The primary characteristics illustrated by such an experiment are 1) extreme nonlinearity in the stress-strain dependence; 2) hysteresis (*i.e.*, the behaviour depending on stress history); and 3) the material exhibits *discrete memory* (also called *end point memory*) (*e.g.*, [1]). Discrete memory can be described as follows. If a partial stress cycle is conducted during the quasistatic cycle (*e.g.*, small loops inside the big loop in fig. 3c), the outer (low frequency) loop is maintained; discrete memory is a memory

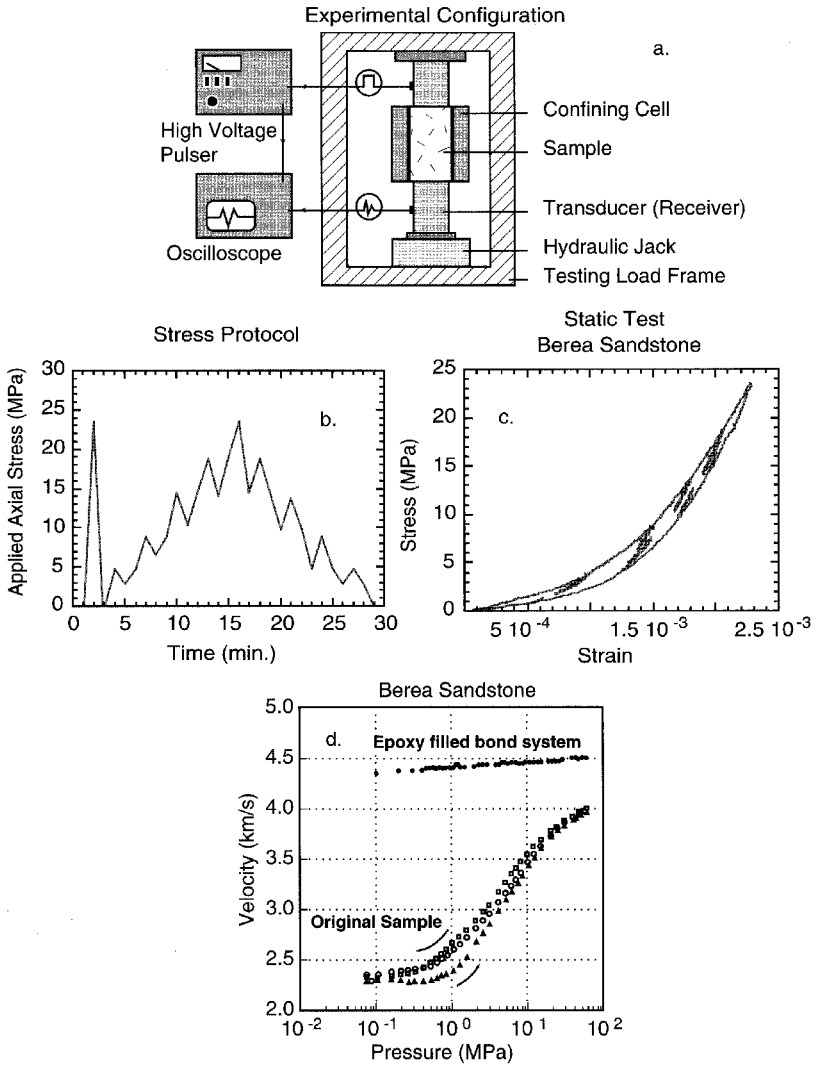

Fig. 3. – (a) Typical experimental configuration for a static stress-strain experiment along a single axis (uniaxial). (b) Stress history or "protocol" for the stress-strain data shown in (c). (c) Stress-strain experimental result for sandstone. The plot illustrates a nonlinear stress-strain relation, hysteresis, and end point (discrete) memory. (d) Velocity *vs.* pressure results from Gist [18]. The open characters represent data taken before the epoxy injection. The triangles are the first upward pressure cycle, the squares are the first downward pressure cycle, and the circles are the next upward cycle (this is the normal quasistatic conditioning observed in this type of experiment due to elastic and plastic deformation). The dark circles show the result after the flat pores (the bond system) are filled with epoxy. As a result, the hysteresis in pressure-velocity disappears, and there is almost no velocity dependence on pressure.

of the previous maximum strain state. Similar results have been obtained by numerous researchers, *e.g.* [16, 17, 14].

The origin of the hysteresis and discrete memory is in the bond system, as Gist [18] and Zinszner (unpublished) have shown. In their experiments, a rock sample was tested in a quasistatic experiment similar to that shown in fig. 3a. During the pressure test, velocity was measured by the time delay method or by resonance. Next, the sample was placed in vacuum, and liquid epoxy was injected into it. Following this, the sample was spun in a centifuge to eliminate epoxy from the rounded pores. The quasi-static experiment was then repeated, and the hysteresis and dependence of modulus with pressure nearly disappeared. The results from Gist are shown in fig. 3d.

The manifestations described above have important consequences for the material elastic modulus because the modulus is the derivative of the stress with the strain, $\partial\sigma/\partial\epsilon$. In short, static tests indicate that the value of the modulus depends on the stress history and the current EOS amplitudes, and changes discontinuously at the stress strain cusps. This is a well-known but underappreciated observation.

2·2. *Dynamic indicators.* – There exist numerous methods by which to observe nonlinear effects. In the acoustics of liquids and gases, the harmonics of a periodic travelling wave can be monitored out to the distance of shock wave formation. However, for relatively low-frequency and low-amplitude sound in solids, it is difficult to obtain quantitative results from travelling wave experiments due to strong wave dissipation and to the fact that one cannot easily make measurments at arbitrary points in the media, as in liquids. Nonetheless, travelling wave measurements are important, *e.g.*, for parametric array development and nonlinear imaging.

The majority of quantitative measurements for rocks have been performed with resonant bar experiments. Due to the amplification that resonance provides, it is perhaps the most sensitive manner by which to observe nonlinear behaviour, even at extremely small dynamic strains, as small as $\epsilon = 10^{-9}$. (In a simple one-dimensional configuration, $\epsilon = \partial u/\partial x$, where u is the displacement.)

Quantitative indicators of nonlinear behaviour from dynamic experiments in solids are based on the relation between the detected strain amplitude of the drive frequency and the following: 1) harmonic amplitudes, 2) wave cross-modulation amplitudes, 3) resonance frequency shift, and 4) amplitude-dependent losses. Lastly, 5) the slow dynamical nonlinear response is used as a quantitative indicator. It is the observation of these effects that indicates that the material is behaving nonlinearly and may tell us about the nature of the nonlinearity, for instance, whether or not nonclassical behaviour such as hysteresis is present in dynamic processes. In the following we outline these quantitative nonlinear indicators.

2·3. *Nonlinear resonance frequency shift.* – Resonance frequency shift is a sensitive measure of the amplitude dependence of the resonance frequency that can be used for calculation of the average modulus and wave speed. A typical 1-D resonance experimental configuration for obtaining amplitude at the bar end *vs.* wave drive frequency (*e.g.*, [19] and [20]) is shown in fig. 4. Measurements are normally made of both upward and downward swept frequency response over a frequency interval that contains the fundamental mode resonance. Typically, tens of frequency sweeps are repeated at successively increasing drive voltages over the same frequency interval in order to monitor resonant peak shift. Acceleration is frequently measured from which strain is calculated.

Figure 5a shows resonant bar results from an atomic elastic material (polyvinylchlo-

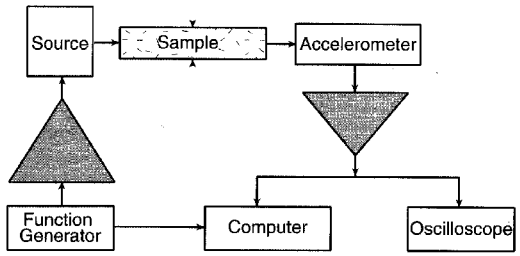

Fig. 4. – Experimental configuration for resonance bar experiments.

ride, PVC) having a quality factor Q similar to many rocks ($Q = 59$). The figure shows detected acceleration *vs.* swept frequency. Both downward and upward resonant sweeps were conducted at each drive level. Figure 5b shows a representative result for nonlinear

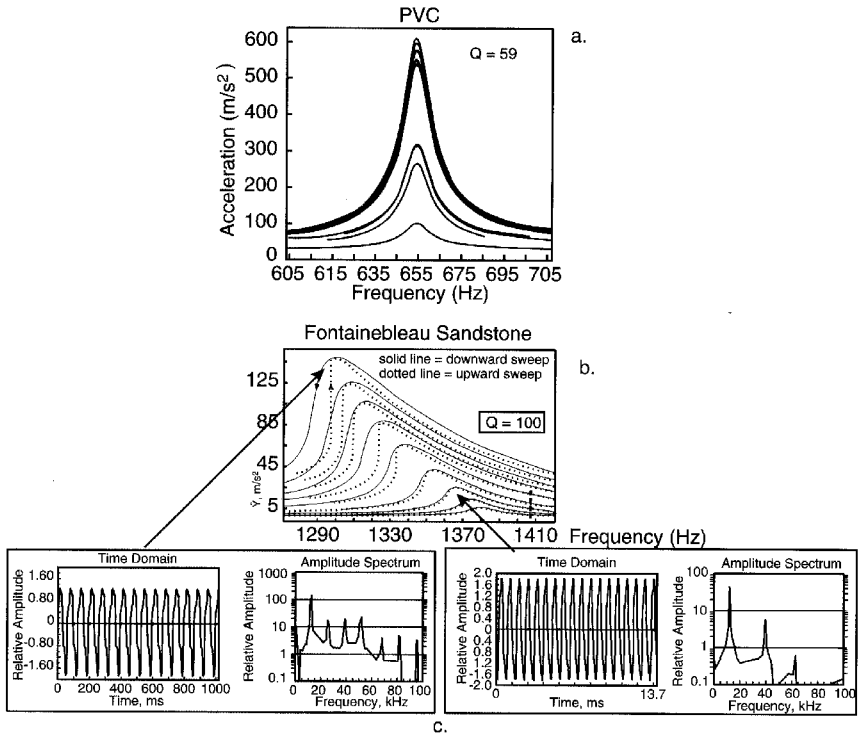

Fig. 5. – (a) Resonance acceleration response of polyvinylchloride (PVC) for several drive levels. (b) Resonance acceleration response of Fontainebleau sandstone, for increasing drive. (c) Time and frequency domain signals from relatively low amplitude, but nonlinear, drive levels (right), and at large drive levels (left). The time signals are obtained at peak resonances in each case.

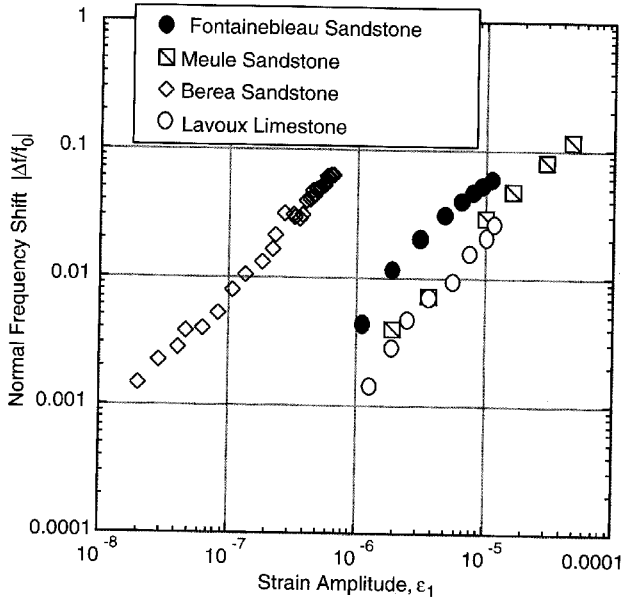

Fig. 6. – Normed frequency shift ($(f - f_0)/f_0$, where f_0 is the linear resonance peak) *vs.* strain amplitude for various rocks under various experimental conditions. Slope of approximately one indicates that nonclassical nonlinearity is responsible for the peak shift.

resonant behaviour in a rock [19]. The material is Fontainebleau sandstone under ambient temperature and pressure conditions. The solid and dotted lines in fig. 5b indicate that the resonance response is dependent on the direction of the frequency shift (up or down). This is a manifestation of slow dynamical behaviour. Figure 5c shows the time and frequency response at relatively small (right) and large amplitudes (left), respectively. Clearly the intensity of the distortion increases significantly with wave amplitude.

By plotting the frequency shift as a function of the fundamental-mode strain amplitude, we can infer key information about the nature of the nonlinearity, and, based on the appropriate model, extract the nonlinear coefficients. For example, fig. 6 illustrates such a result for various rocks. The dependence between the detected frequency shift and the strain has a power law relation of one in all cases. This is unexpected behaviour for classical nonlinear acoustics where this dependence is quadratic, and implies that hysteresis is present at not only the static forcing level as we saw earlier, but the dynamic level for small strains. We will address this issue further.

A complementary series of experiments was performed by Nazarov *et al.* [21]. A typical experimental configuration is shown in fig. 7a. The measurements were performed in samples 30 cm × 8 mm × 8 mm composed of granite and for a cylinder 20 cm long and 5 cm in internal diameter, filled with a wet sand; the latter was exposed to intensive sound over 4 hours to obtain stable results. Figure 7b shows the resonance frequency shift for these materials as a function of exciting strain ϵ_0. As with the data shown in fig. 6, the shift is linearly proportional to ϵ_0 for the granite and the sand. Of significance is that

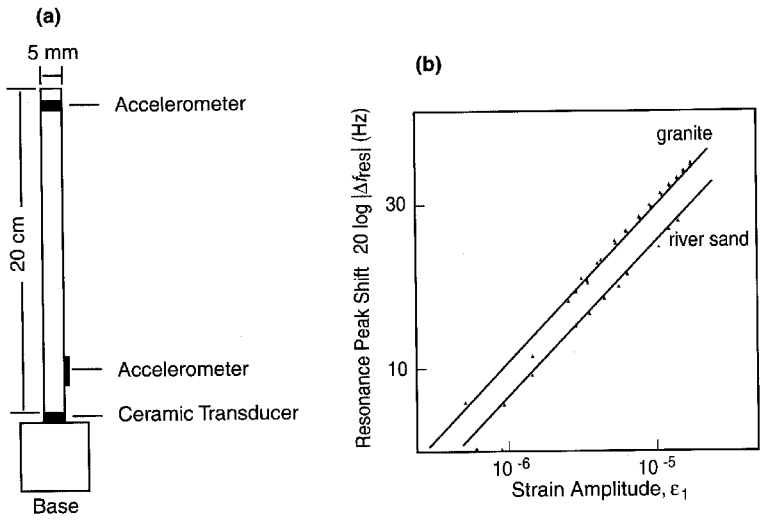

Fig. 7. – Resonance experiments in wet sand (grain diameters of about 0.3 mm) and granite. (a) experimental setup. (b) Resonance peak shift *vs.* strain amplitude ε_1. The excitation frequency was 3.6 kHz (first-mode resonance) $[\Delta f = f - f_0]$.

these are some of the very few existing measurements in unconsolidated material, the sand, and they show the same dependence with strain as the rocks. (Notably, Nazarov found a different dependence in another material, marble. This may be due to the influence of slow dynamics, which can significantly affect this type of measurement.

2·4. *The effect of fluids.* – Nonlinear experiments in sandstone and limestone at partial water saturation show that nonlinear response has a stronger dependence on the presence of water than the linear characteristics, wave speed and dissipation [22], for example. Figure 8a shows resonant frequency shifts for Lavoux limestone, conducted at water saturations ranging from 1% to 98%. The nonlinear response in fig. 8, as measured by the change in resonant frequency *vs.* strain, shows nearly an order of magnitude increase from 1–25% saturation. For higher saturations, the response remains approximately the same. Fluids complicate the nonlinearity significantly due to capillary forces and their effect on the matrix and pore space. These effects are well described in Van Den Abeele *et al.* (2000) [22], see also [81].

2·5. *Slow dynamics.* – Another important characteristic of nonclassical materials is slow dynamical (relaxation) response. Slow dynamics in this context means that the average material modulus is temporarily altered (lowered) during wave excitation. After wave excitation, it takes some time (order 10^3 seconds) for the material modulus to recover to its original state. One manner in which to observe this behaviour is to monitor the resonance frequency before and after large excitation (*e.g.*, [23, 24]). That is, after measuring the linear resonant peak, the sample is driven at large amplitude for several minutes. The low-amplitude resonant peak is then monitored until the resonant peak has

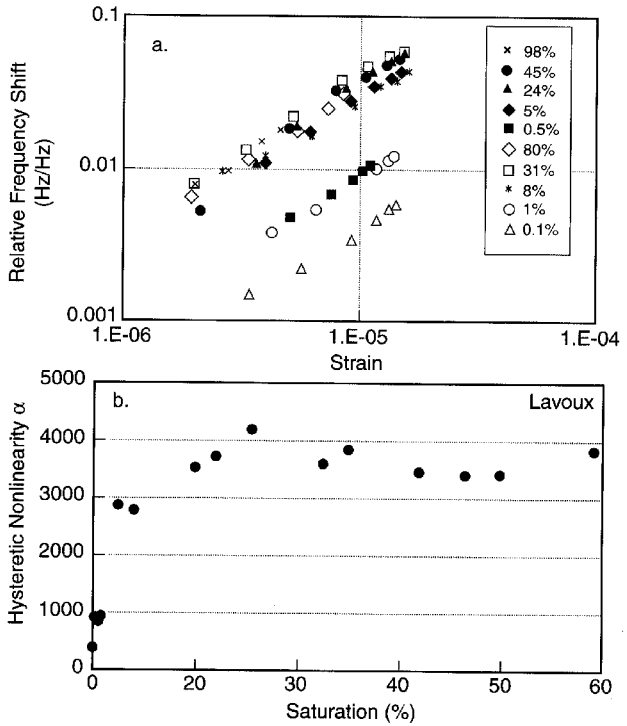

Fig. 8. – (a) Resonance frequency shift as a function of strain amplitude at different water saturations (in percent) in Lavoux limestone. (b) Nonlinear coefficient α (see eq. (8) below) as a function of saturation obtained from the data in (a).

returned to its original frequency. An example of slow dynamics is illustrated in fig. 9 for several different rock types and for concrete. The slow dynamical scaling of the resonance frequency recovery in time is logarithmic [24]. This result has important consequences regarding the origin of the nonlinear response (to be addressed). In recent work [25] it has been discovered that damaged atomic elastic materials also display slow dynamics. The class of materials displaying slow dynamics is expanding rapidly. An important aspect regarding slow dynamics is that if it is observed, the other manifestations of nonlinear response are observed as well (wave mixing, resonance peak shift, etc.).

2·6. *Harmonic generation.* – A large series of experiments of the type shown in fig. 4 have dealt with measurement of harmonic amplitudes via Fourier analysis [19]. The slopes of the second and third harmonic amplitudes with the strain amplitude of the fundamental provide further quantitative information about the nature of the nonlinearity. For instance, a typical result for Berea sandstone is shown in fig. 10a. The fact that the second- and third-harmonic amplitude slopes are nearly identical also indicates that classical nonlinearity is not sufficient to explain such behaviour.

The amplitude dependences of second and third harmonics obtained in the experiment

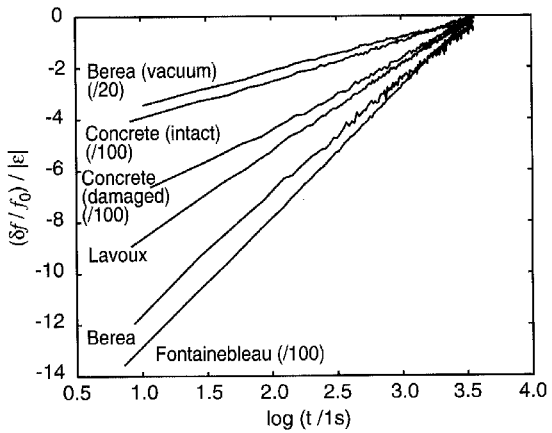

Fig. 9. – Slow dynamical response in several rock types and in concrete. The time-dependent shift δf of the recovering resonant frequency, normalised to the asymptotic value f_0, per unit driving strain $|\epsilon|$. Sample names are indicated in the figure, and some scale shifts were divided by the indicated factors for plotting. Lavoux is a limestone, Berea and Fontainebleau are sandstones, and one sample of concrete was more damaged than the other (damaged *vs.* intact, respectively).

in fig. 7a [21] are shown in figs. 10b and 10c, respectively, for granite and wet sand. These results further indicate that the EOS is nonanalytic, and again that unconsolidated material behaves like rock.

Most experiments have been conducted in Young's mode resonance, however, some torsional measurments have been conducted as well by Bonner and colleagues at Lawrence Livermore National Laboratory in California [26, 63]. The results of this work support a hysteretic model of the EOS [27].

2·7. *Wave modulation experiments.* – A simple wave modulation experiment is conducted as follows. Two single-frequency, continuous waves, one of high and another of low frequency (fig. 11a), are excited in the sample as illustrated schematically in fig. 11b. The sample acts as a nonlinear mixer (multiplier), so that the sum and difference-frequency waves (sidebands) are created, in addition to harmonics, as illustrated in figs. 11c, d.

Figure 11e illustrates an actual experiment in Berea sandstone. The plot shows the increase in amplitude at second-sideband frequencies as the drive intensity at one input frequency is increased (the other was held at fixed amplitude). The dependence, which is the same as for the first side-band amplitude (not shown), once again indicates nonclassical nonlinearity.

2·8. *Nonlinear dissipation.* – Amplitude-dependent loss is a well-known phenomenon in metals where it is attributed to hysteresis at dislocations. For rocks, for soils and in earthquake studies (*e.g.*, [28]) nonlinear dissipation is nearly always observed, and is an additional indicator of hysteresis in the EOS. Below we mention two examples.

Amplitude-dependent attenuation in earth materials was observed in experiments on nonlinear interaction between low- and high-frequency signals [29, 32]. The experiment was the same as that shown in fig. 7a. During the low-frequency, high-amplitude resonant

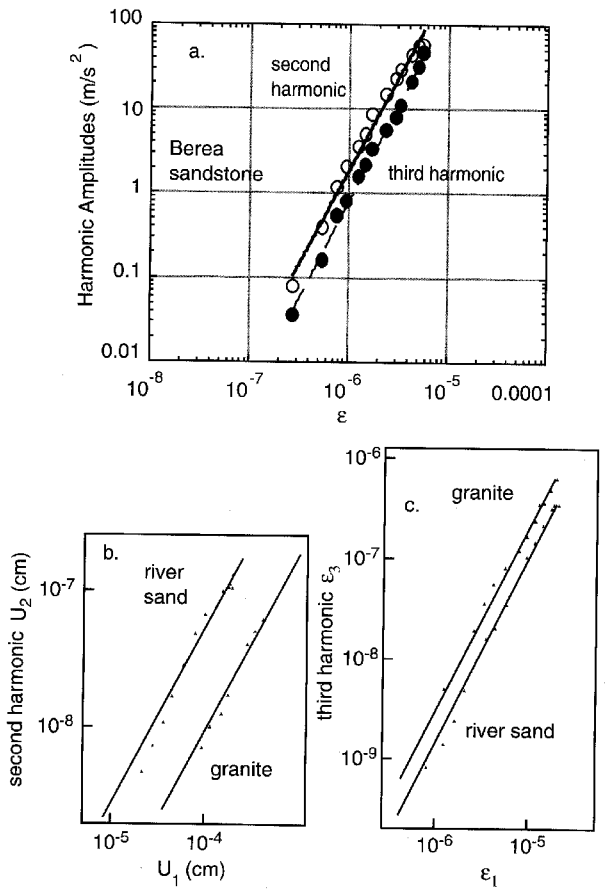

Fig. 10. – (a) Second- and third-harmonic amplitudes as a function of measured strain amplitude in Berea sandstone. The harmonics were obtained from Fourier analysis of the time signal taken at resonance peaks, peaks similar to those in fig. 5b for instance. (b) Dependences of the displacement amplitude of the second harmonic U_2 on the fundamental displacement amplitude U_1 in river sand and granite. (c) Dependences of the amplitude of the third harmonic ϵ_3 on the fundamental strain amplitude ϵ_1 in river sand and granite. The fits correspond to a power law relation of 2 for both materials, indicating nonclassical nonlinearity.

excitation ("pump wave"), a longitudinal ultrasound pulse (frequency 200 kHz, pulse duration 70 ms) was generated to propagate for some distance along the bar, after which its amplitude was measured and the spatial damping rate was calculated. In the presence of the low-frequency mode, the ultrasound damping rate increased in proportion to the low-frequency strain amplitude ϵ_1 in granite and sand, and to ϵ_1^2 in marble (fig. 12). This is also the effect of dissipative nonlinearity. Note that the observed effect was reversible.

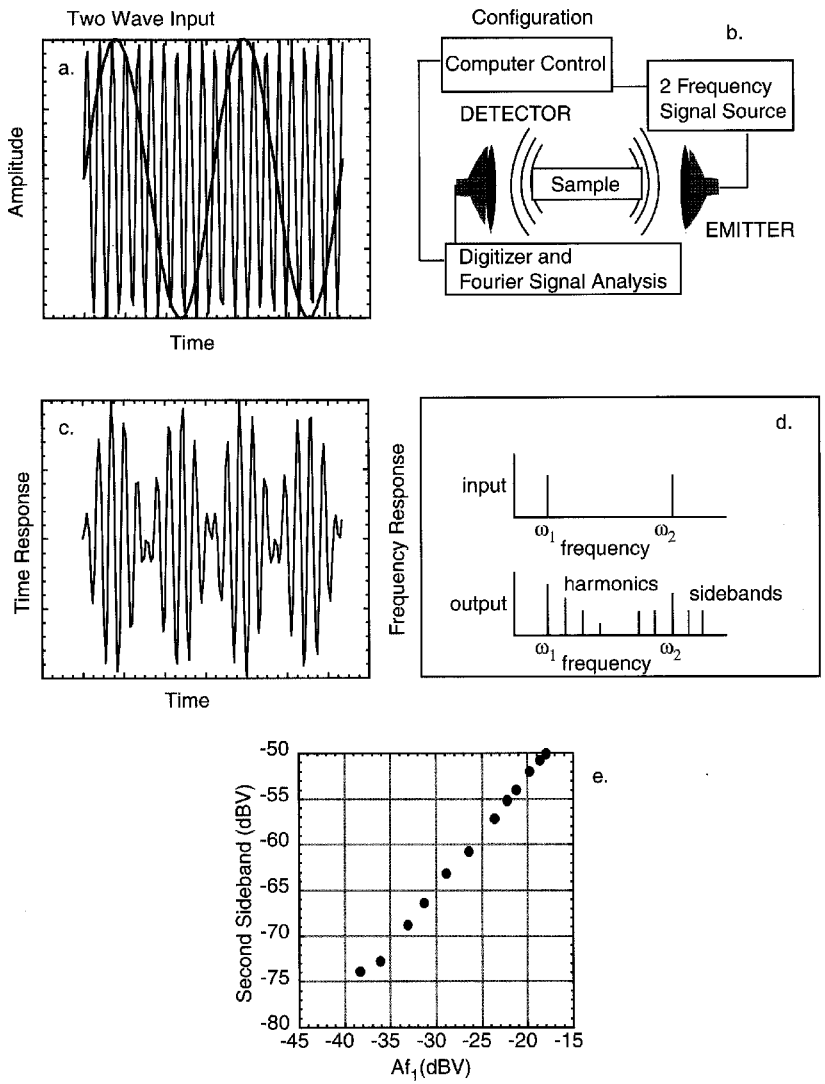

Fig. 11. – Typical wave modulation experiment. (a) Two pure-tone sinusoidal inputs at two separate frequencies. (b) Experimental configuration. (c) The time-series output due to nonlinear mixing in the sample. (d) The spectral response of the time signals in (a) and (c). Sidebands of at least first order ($f_2 \pm f_1$) and second order ($f_2 \pm 2f_1$), as well as harmonics appear. (e) The dependence of the second sideband amplitude on the amplitude of one of the two fundamental frequencies in Berea sandstone, indicating nonclassical nonlinearity.

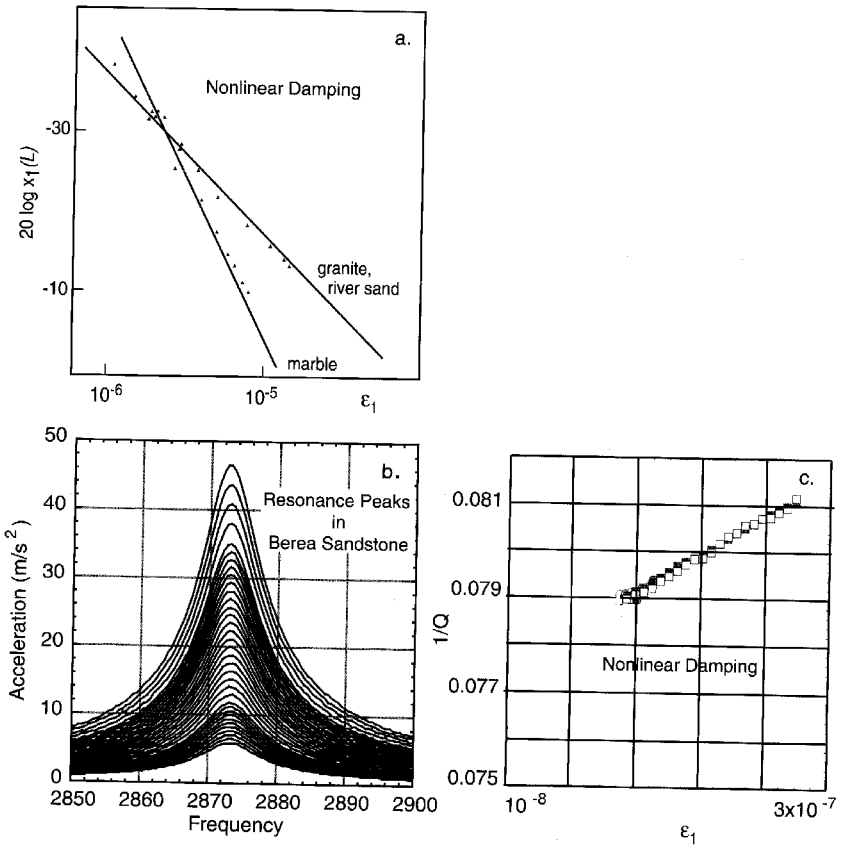

Fig. 12. – Nonlinear damping. (a) From the experimental configuration described in fig. 7, dependence of the coefficient of nonlinear damping of a 200 kHz ultrasound pulse ($X_1(L) = \ln[A_0/A(L)]$, where A_0 is the amplitude of the input pulse without the "pump" wave, $A(L)$ is the output amplitude of the rod) on the amplitude ϵ_1 of the low-frequency resonance "pumping" wave for three materials. For the sand and granite, the dependence is $X_1(L) \propto \epsilon_1$; for the marble $X_1(L) \propto \epsilon_1^2$. (b) From the experimental configuration described in fig. 4, resonance acceleration amplitude *vs.* frequency at very small acceleration levels. (c) From the data in (b), $1/Q$ (attenuation) *vs.* strain. Note that, even for very small strain levels, nonlinear attenuation exists in this sample (the nonlinear frequency shift, albeit small, is present as well).

Similar experiments for control samples (glass) did not reveal any significant nonlinear effects.

Figures 12b, c show results from a resonance experiment in Berea sandstone [20] under vacuum conditions at very small acceleration and strain levels like that shown in fig. 4. In the resonance data shown in fig. 12b, a very small frequency shift and peak broadening can be observed. Figure 12c shows the actual change in $1/Q$ extracted from 12b. It is

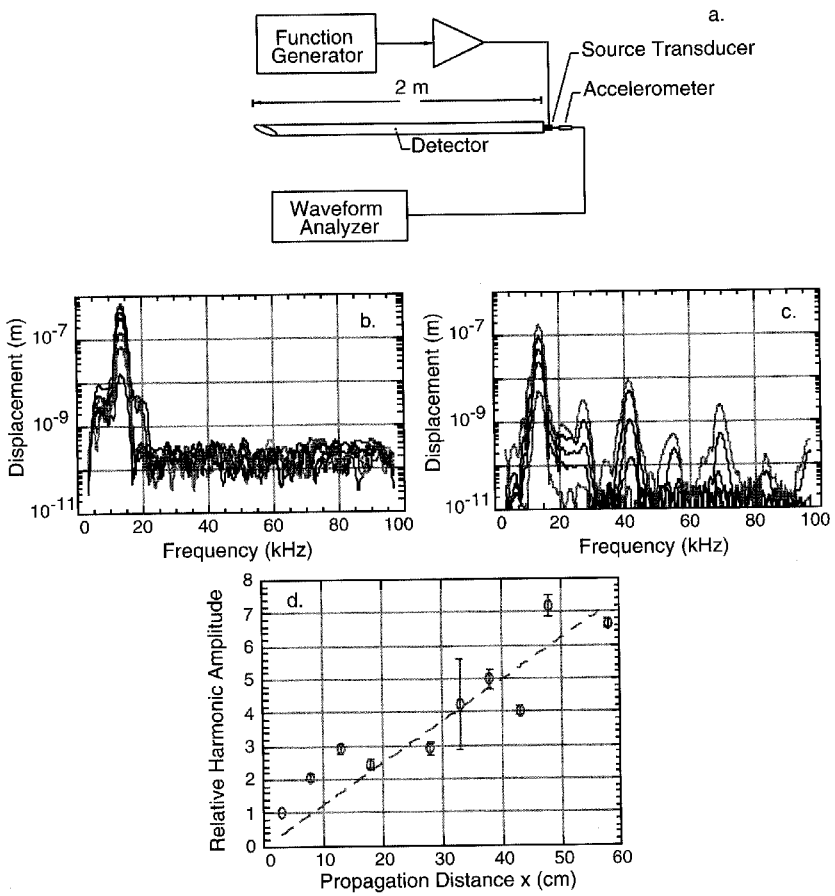

Fig. 13. – (a) Experimental configuration for pulse-mode experiments. The source transducer emits a tone burst and an accelerometer measures the characteristics of the tone burst at the source. Detectors placed at various distances measure the spectral evolution of the time signal. Numerous detectors were either embedded in the sample or placed on the surface, depending on the experiment. (b) Source displacement spectra for a 13.75 kHz drive toneburst. Observations for progressively increasing drive level are illustrated by the various lines. (c) Displacement spectra after the wave has propagated 58 cm for a drive at 13.75 kHz. Line types correspond to those in (b) and illustrate progressive growth of harmonic amplitudes with source amplitude. (d) Normalized (linear attenuation eliminated) second-harmonic displacement amplitude as a function of distance. Error bars indicate uncertainty of measurement amplitude.

remarkable that nonlinear attenuation can occur at such small strain levels. In order to extract the attenuation from data collected at such small strain amplitudes, Guyer developed a method called "Constant Strain Analysis" which can be applied universally to small-strain, resonance data.

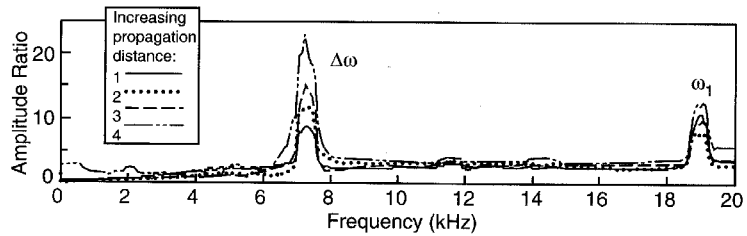

Fig. 14. – Spectrum showing difference frequency ($\Delta\omega$) growth at four distances (2, 4, 8 and 16 cm from the source) in a pulse mode experiment similar to that shown in fig. 13a. Darker bold lines respresent successively further distances from the source. The input frequencies are 19 (ω_1) and 26 kHz, so the difference frequency is 7 kHz. (Unpublished results from Johnson and Meegan, 1993.)

2·9. *Experiments with travelling waves.* – The cumulative character of nonlinear wave evolution can be observed from the variations of a travelling wave during propagation. For instance, an experimental observation of the spectral evolution of a travelling wave as a function of distance for an initially narrow-band acoustic impulse [33] is illustrated in fig. 13. In order to account for transducer contact effects (source effects) and linear attenuation, a spectral ratio method was applied. In fig. 13d, the relative harmonic amplitude is obtained by taking the ratio of the second-harmonic amplitude to the amplitude of a linear elastic wave input at the same frequency $2f$. In this way the linear attenuation and possible source nonlinearity effects have been eliminated. The higher-harmonic displacements have amplitudes that are a sensitive function of the drive amplitude and propagation distance (see eq. (25) below).

Another similar experiment is difference-frequency wave generation by interaction of two high-frequency waves, as in the parametric array mentioned above. The first published laboratory result demonstrating a parametric array in earth solids was from the Los Alamos group who developed the Frequency Domain Travel Time method for extracting the difference-frequency wave out of noisy data [34]. From later work applying an experiment similar to that described in fig. 13a, fig. 14 shows the evolution of the frequency spectrum of the low-frequency field with distance from the two-frequency source (normalized to eliminate the effects of linear dissipation), that increases with distance, as predicted by theory (unpublished data from Johnson and Meegan).

Directivity of an analog of a parametric array in a solid is shown in fig. 15. The beam intensity pattern of a difference frequency wave measured at a fixed distance from the source shown in fig. 15a, with the beam patterns of the primary wave frequencies shown in fig. 15b.

Another observed effect is "self-demodulation", also well known in nonlinear acoustics. This is a parametric array-type effect as well, where a high-frequency tone burst (also known as a carrier wave) produces a low-frequency component by nonlinear interaction in the course of propagation. Eventually all that is left of the tone burst is a squared and differentiated version of the original envelope function ("video" pulse). All of the high frequency dissipates. Zaitsev *et al.* [35] excited a high-frequency (180 kHz) pulse in dry and wet river sand, and obtained a self-demodulated wave (fig. 16-1) and provided a theoretical description.

Figure 16-2 shows a result of a pulse-mode experiment by Johnson and McCall [36]

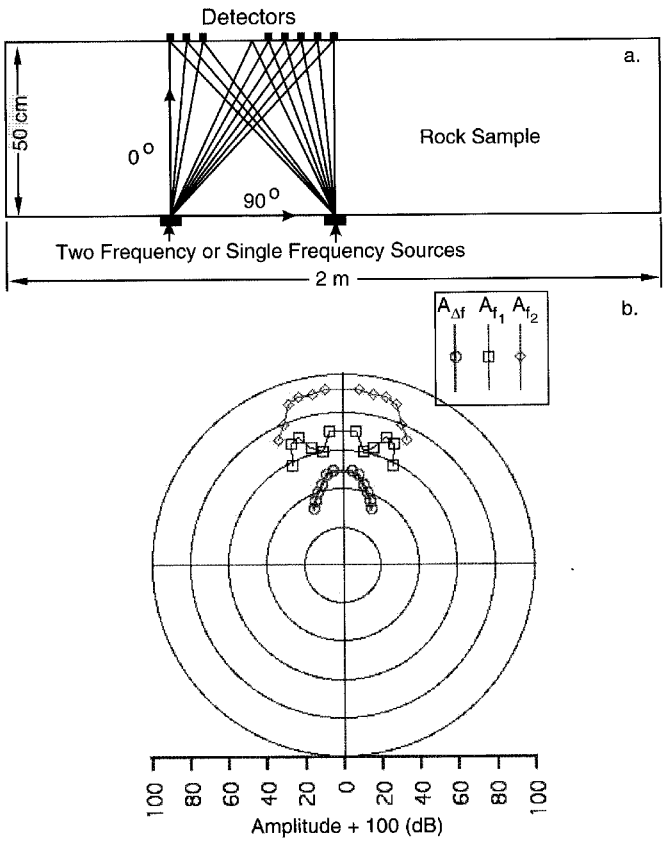

Fig. 15. – Beam pattern of collinear difference frequency formed by parametric interaction in Berea sandstone. (a) Geometry of the block of sandstone (the thickness of the sample was 0.5 m), the location of the source and detecting transducers and the raypaths. To minimize the number of detectors used in the experiment, two source positions were used to obtain both sides of the beam pattern. (b) Polar plot showing comparison between the difference-frequency signal created in the rock by nonlinear interaction (parametric array) shown as $A_{\Delta f}$, and the primary wave beam patterns, A_{f_1} and A_{f_2}. The beam pattern is shown as iso-intensity (in dB) *vs.* the angle from the axis of the source. Zero degrees corresponds to the shortest raypath, directly across the sample. The high-frequency waves were in the range of 200 kHz, and the difference frequency was approximately 7 kHz (from Johnson and Shankland 1991, unpublished).

identical to that shown in fig. 13a conducted using a broad frequency-band source in a sandstone bar. (This experiment is an analog of the well-known Pestorius-Blackstock experiment in air [37].) For detected displacements at the fundamental frequency as small as $3 \cdot 10^{-8}$m, the composition of the displacement frequency spectrum at 1 m is extremely rich in frequencies that are not present at the source. As drive amplitude is increased, the spectrum becomes progressively richer (broader) due to the nonlinear

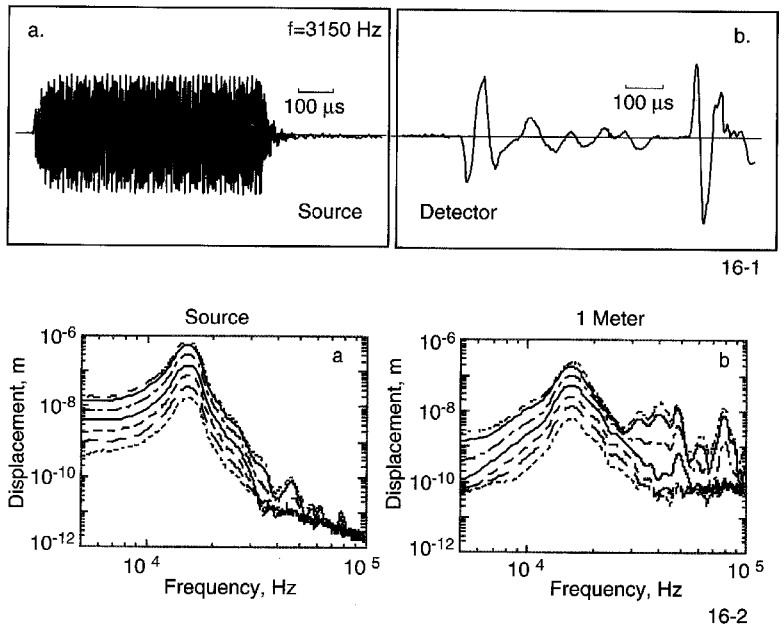

Fig. 16. – 1. Self-demodulation of a high-frequency pulse in sand under the static pressure of 9000 Pa. (a) Time series of a primary wave, and (b) detected pulse. 2. Broadband displacement spectra from pulse-mode experimental studies from an experimental configuration identical to that shown in fig. 13a. The source signal is a Blackman window of peak frequency, approximately 20 kHz and the signal is band-limited at 7 and 32 kHz. (a) The source displacement spectrum at successively increasing applied voltages. (b) Displacement spectrum 1 m from source at increasing applied voltages corresponding to drive levels in 16-2a. Note the increased complexity of the spectrum at larger drive levels for the signal at 1 m.

elastic wave interaction in the material. This experiment has potential applications to seismic waves, especially the near-source waves.

2·10. *Noncollinear interactions of acoustic beams.* – Rollins *et al.* [38] demonstrated that pulse-mode body waves could interact at angles in solids, and produce sum and difference frequency waves, based on the resonance conditions (selection rules) well known in nonlinear optics and acoustics. *E.g.*, for a "three-wave interaction" with frequencies $\omega_{1,2,3}$, and the respective wave vectors $\mathbf{k}_{1,2,3}$ these conditions are $\omega_1 + \omega_2 = \omega_3$ and $\mathbf{k}_1 + \mathbf{k}_2 = \mathbf{k}_3$. That is possible if waves of different types are interacting, for instance, two compressional and one shear wave. This type of wave mixing is also known as noncollinear wave interaction. The Rollins *et al.* experiment was duplicated in several experiments with rock [39, 40] where two compressional waves interact to create a shear wave. Figure 17a, b shows the experiment and results of such an experiment conducted on a sandstone sample, for a fixed interaction angle, while progressively altering the input wave frequency ratio. The selection rules derived from the nonlinear wave equation indicate that only one frequency ratio will optimize the Δf mixing, and the peak am-

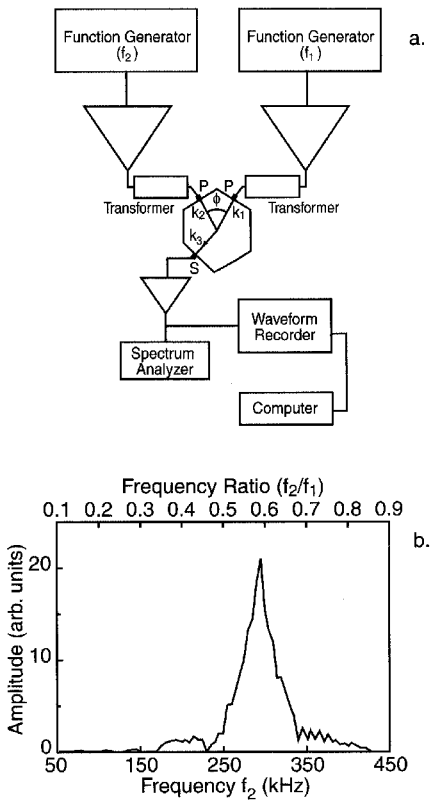

Fig. 17. – Noncollinear wave interaction. (a) Block diagram of experimental configuration used in noncollinear wave experiments for the case of two compression waves interacting to create a shear wave. k_1, k_2, and k_3 are wave numbers, and ϕ illustrates the input wave interaction angle. P and S refer to compressional and shear wave transducers, respectively. (b) Noncollinear wave experimental result. Amplitude dependence of the difference frequency beam as a function of drive frequency f_2 for Berea Sandstone. f_2 is swept over a frequency interval from 50 to 450 kHz, and the drive frequency f_1 is fixed. The predicted peak amplitude should occur at $f_2/f_1 = 0.61$, or $f_2 = 305$ kHz. The observed peak occurs at $f_2/f_1 = 0.59$ (295 kHz). The slight discrepancy is due to the anisotropy of the material, not accounted for in the prediction.

plitude value of the created shear wave is that predicted by the selection rules. This configuration can be used for imaging of specific volumes in the interior of materials.

3. – Theoretical models

From the above measurements one can calculate a set of fundamental nonlinear parameters of the material and attempt to use them in order to infer the nature of the nonlinear response, and to create models. A theory must correctly predict 1) the static hysteresis and discrete memory, 2) the resonance frequency-strain amplitude dependence, 3) the second- and third-harmonic amplitude variation with the fundamental amplitude, 4) the first- and second-order sideband scaling from wave modulation, and 5) the logarithmic dependence of slow dynamics. The full theory of these effects has not been constructed yet. However, the models and approaches described below provide at least a qualitative explanation of much of the experimental evidence.

3·1. *Classical theory.* – The classical nonlinear theory for atomic elasticity is thoroughly described in the literature (*e.g.*, [41]), and we will provide only a brief overview. The classical theory begins with the expansion of the elastic strain energy in powers of the strain tensor, ϵ_{ij}. The expansion coefficients designate the components of the second-order elastic tensor and the third-order elastic tensor. These tensors are characterized, respectively, by 21 and 56 independent components for an arbitrary anisotropic medium (in the lowest-order, triclinic material symmetry) and by only 2 and 3 components, respectively, in the highest-order symmetry (isotropic material).

The equation of motion in Lagrangian coordinates is

$$\rho \ddot{u}_i = \frac{\partial \sigma_{ij}}{\partial x_j}, \tag{1}$$

where u_i are the components of the displacement vector, $\mathbf{u}$, and ρ, σ_{ij} and $\ddot{u}$ designate the density, the stress tensor and the particle acceleration, respectively.

To gain insight one can consider the one-dimensional case. For a longitudinal wave (P-wave) propagating in an isotropic medium, a one-dimensional wave can exist with only nonzero components $\sigma_{xx} = \sigma$ and $u_x = u$ or $\epsilon_{xx} = \epsilon = \partial u/\partial x$. The corresponding equation of motion can be written as

$$\rho_0 \frac{\partial^2 \epsilon}{\partial t^2} = \frac{\partial^2 \sigma(\epsilon)}{\partial x^2}. \tag{2}$$

From the energy expansion, the stress-strain relation (also known as the equation of state, or EOS) can be written as

$$\sigma = M\left(\epsilon + \beta\epsilon^2 + \delta\epsilon^3 + ...\right), \tag{3}$$

where M is the elastic modulus (for a bar it coincides with the Young modulus, E), and β and δ are nonlinear coefficients that can be expressed in terms of combinations of the elastic moduli (*e.g.*, [42]). For example, the nonlinearity parameter β can be expressed in terms of Landau moduli, A, B, C, or Murnaghan moduli, l, m, n:

$$\beta = \frac{3}{4} + \frac{A + B + C}{2\rho c^2} = \frac{3}{2} + \frac{l + 2m}{\lambda + 2\mu}. \tag{4}$$

Here λ and μ are so-called Lame coefficients. A typical order of these parameters for atomic elastic solids is 10^{11}–10^{12} Pa.

From (3) it follows that the local sound velocity is

$$c = \sqrt{\rho^{-1} \mathrm{d}\sigma/\mathrm{d}\epsilon} \approx c_0(1 + \beta\epsilon + (3\delta - \beta^2)/2\epsilon^2 + ...). \tag{5}$$

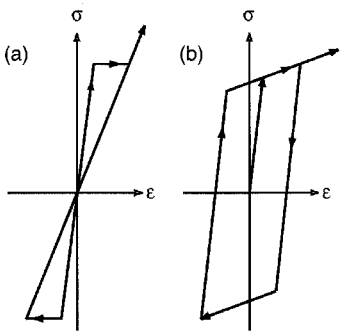

Fig. 18. – Two nonclassical models of the EOS from Asano (1970). (a) "Ratchet" model. (b) "Slider" model.

It is important to note that even if the nonlinearity is anomalously large in earth materials in comparison with that of atomic elastic media, the nonlinear terms in the EOS are generally much smaller than the linear term. This is because ϵ is of order 10^{-5}–10^{-9} in dynamic experiments. Therefore, one can use relation (3) and its generalizations for media with strong nonlinearity but only if hysteresis is not significant.

This nonlinearity can be caused by two mechanisms. The first is of a "geometrical" or "kinematic" type, related to the difference between the Lagrangian and Eulerian descriptions of motion. The other type is "physical" elastic nonlinearity. Physical nonlinearity is described by third-order (and higher-order) terms in the expansion of the elastic energy in ε, and accounts for the fact that stress is not a linear function of strain. Geometrical nonlinearity is typically comparable in order to physical nonlinearity in atomic elastic materials, such as fluids and intact solids. In rock and other highly nonlinear media physical nonlinear response is typically orders of magnitude larger than geometric nonlinear response, and therefore, the latter can be ignored.

3·2. *Phenomenological models with hysteresis.* – Since the mechanisms of nonlinear response in hysteretic materials are not well understood yet, phenomenological models have been appealed to. Here, we illustrate some models that successfully describe the behaviours shown earlier.

An adequate equation of state must include the dependence on the history of the process which can be characterized by the sign of $\dot{\epsilon} = \partial\epsilon/\partial t$:

$$\sigma = M\left(\epsilon + \beta\epsilon^2 + \delta\epsilon^3 + ...\right) + \hat{S}\left[\epsilon, \mathrm{sign}(\dot{\epsilon})\right], \tag{6}$$

where $\hat{S}$ is a function describing "nonclassical" effects. A specific form of $\hat{A}$ should follow from the material physics. In an early work by Asano [43] two basic types of the nonclassical (hysteretic in stress-strain) behaviour were considered. One of them is of a "ratchet" type: it starts from zero point on the (σ, ε)-plane, and has a "butterfly" shape; it is related to the Granato-Lücke model discussed below. The second, a "slider", starts from zero in stress-strain space as well, but for a periodic motion surrounds this point (fig. 18, a and b). If these elements are distributed in sizes, these curves become smooth (see the examples below) but still preserve the same topologies. In many cases these

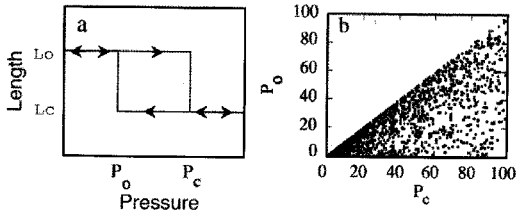

Fig. 19. – (a) Hysteretic Elastic Unit (HEU) in length-pressure space. (b) Typical PM-space representing the density of HEUs in a sample for a rock.

forms were introduced as a "best fit" for experimental values and dependences. One example (of the first type) is the following [21]:

$$\hat{S} = \begin{cases} \epsilon - (\beta_1/2)\epsilon^2\,; & \epsilon > 0\,, \quad \partial\epsilon/\partial t > 0\,, \\ \epsilon\left[1 - \epsilon_0\left(\beta_1 + \beta_2\right)/2\right] + \left(\beta_2/2\right)\epsilon^2\,; & \epsilon > 0\,, \quad \partial\epsilon/\partial t > 0\,, \\ \epsilon + (\beta_3/2)\epsilon^2\,; & \epsilon < 0\,, \quad \partial\epsilon/\partial t < 0\,, \\ \epsilon\left[1 - \epsilon_0\left(\beta_3 + \beta_4\right)/2\right] - \left(\beta_4/2\right)\epsilon^2\,; & \epsilon < 0\,, \quad \partial\epsilon/\partial t > 0\,, \end{cases} \tag{7}$$

where ϵ_0 is the strain amplitude and β_i are the nonlinearity parameters. Using this EOS enabled the authors to describe nonlinear indicators from some experiments [32]. However, for other materials the EOS had to be adjusted, so it lacks universal applicability.

The Preisach-Mayergosz Space Model.

A sophisticated model called the Priesach-Mayergoyz space (PM space) model [30], which successfully describes the hysteretic nonlinear behaviour of rock elasticity with discrete memory, was developed in a series of papers by our colleagues [14,44,45,13]. The model is based in part on the work of Holcomb [31] and others who studied memory and relaxation in rock. This model is based on assuming that the elastic properties of a macroscopic sample of material result from the integral response of a large number of individual, elastic elements (of order 10^{12}, a rough estimate of the number of grain-to-grain contacts, microcracks, etc., in one cubic centimetre of rock). Each elastic element may or may not demonstrate hysteretic behaviour. The individual elements are combined for analysis in what is known as PM space.

Figure 19a illustrates the behaviour of a single elastic element, called a hysteretic elastic unit (HEU), which is characterized by a rectangular length-stress dependence. A large number of such elements with different parameters L_o, L_c, σ_o, and σ_c (length open and closed, stress open and closed, respectively) constitute a model of the compliant portion of a sample material. A plot of (σ_c, σ_o) pairs (L_c and L_o) is the basis of PM space as shown in fig. 19b. The corresponding model material is composed of a large number of HEUs, which exhibit varying degrees of hysteresis that can be seen in PM space. Nonhysteretic units fall on the diagonal and hysteretic units fall below the diagonal, $\sigma_o < \sigma_c$. The more hysteretic an HEU is, the farther from the diagonal it resides. If no hysteresis is present, all elements fall on the diagonal, and the model reduces to the traditional theory described above (*i.e.*, $\hat{S}$ in eq. (6) is zero). The density of HEUs in PM space is given as $\rho(\sigma_c, \sigma_o)$.

To obtain an equation of state, two assumptions are made: 1) For the PM space

distribution density, ρ, we take

$$\rho(\sigma_c, \sigma_o) = B(\sigma_c)\hat{\delta}(\sigma_c - \sigma_o) + \alpha, \tag{8}$$

where $\hat{\delta}$ is the delta-function so that B is the PM space density of nonhysteretic HEUs on the diagonal, and α characterizes the distribution of hysteretic elements in PM space. In the presence of a constant prestress $\overline{\sigma}$ (which can be zero) the values of stress, σ, vary from $\overline{\sigma} - \sigma_0$ to $\overline{\sigma} + \sigma_0$, σ_0 being the ambient stress. Also α is assumed a small constant in this interval. The corresponding strain is proportional to the length of an element, $L_0 = L_c - L_o$, which is fixed for all elements.

To obtain the stress-strain relation, we integrate eq. (8). For small acoustic perturbations $\Delta\sigma$, after expanding B in a Taylor series of $\Delta\sigma$, we obtain the dependence $\varepsilon(\sigma)$ in a form of a series and from that, the inverse series $\sigma(\varepsilon)$ in a standard EOS form (6):

$$\sigma = \sigma_0 + K_0\left(1 - r\Delta\sigma\right)\epsilon + K_0\beta\epsilon^2 + K_0\delta\epsilon^3 + \eta\frac{K_0\gamma}{2}\left(\epsilon^2 - \frac{(\Delta\sigma)^2}{K_0^2}\right), \tag{9}$$

where $\eta = 1$ for stress increase and -1 for stress decrease.

The parameters in this equation are related to α and the constants in (9), namely

$$K_0 = 1/B_0L_0\,, \quad \beta = -\frac{B_1}{2B_0}\,, \quad \gamma = -\alpha/B_0. \tag{10}$$

Here B_0 is the zero-order term in expansion of B in σ. The first three terms on the r.h.s. of (9) are a linear response, quadratic and cubic "classical" nonlinearities, respectively. The last term is proportional to α and is due to the presence of hysteretic elements. Note that in the linear approximation, $\Delta\sigma \approx K_0\epsilon$ and the modulus K_0 is of order 10^{10} Pa. For example, at the strain amplitude, ϵ_0, of 10^{-6}, the stress amplitude, $\Delta\sigma \approx K_0\epsilon_0$ is approximately 10^4 Pa (0.1 bar).

Hence, we have a relationship between a "macroscopic" stress-strain relation and the distribution of hysteretic elements that can be helpful for understanding the physics. Schematically in figs. 20a-d we see step-by-step how the model can predict the EOS behaviour of rock from PM space. This model has been successfully applied to describe the static and dynamic nonlinear behaviour noted above (high nonlinearity, hysteresis, discrete memory), see *e.g.*, [14]. The model captures all of the dependences in the harmonics and resonant peak shifts shown earlier, for strains of 10^{-3}–10^{-9} and frequencies from near DC to at least several megahertz. For illustrative purposes, in fig. 21 we compare and contrast typical expected strain dependences of frequency shift, harmonics, and side bands derived from classical theory (eq. (3)) and from the PM space model.

The PM space model remains a phenomenological description that does not contain the physical mechanisms of nonlinear response. Once the mechanism(s) is (are) identified, they can be placed in the model.

4. – Physical models of structural nonlinearity

An adequate physical model of rocks must be associated with their complex structure. As already mentioned, strong nonlinearity is associated with the presence of hard and soft phases, where the soft phase occupies a much smaller volume (up to nanoscale sizes) but it is subject to strong deformation and is the origin of the nonlinear response,

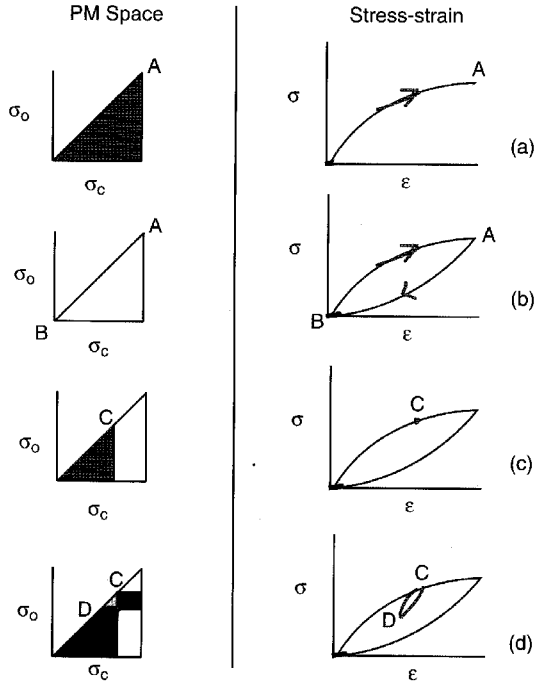

Fig. 20. – Schematic illustrating PM space prediction of stress-strain. In the left-hand column the evolution of the PM space is shown. σ_o and σ_c are the opening and closing pressure of hysteretic units, respectively. In the right-hand column, the corresponding evolution of the stress strain is shown. (a) Evolution from zero pressure to pressure A produces the first half of the full stress-strain curve. All hysteretic units in PM space are closed at pressure A (black region). Following the pressure back to zero pressure at point B, the hysteretic stress-strain curve is constructed. All units in PM space have re-opened (white). (c) The pressure is then taken to point C. All units in black are closed. (d) A small pressure deviation is made, where presssure is decreased to D and then taken back to C. The corresponding loop in stress-strain is formed by this procedure. Closed HMUs in PM space shown in black and open in white.

whereas the hard medium is relatively insensitive to deformation([2]). We call the soft portion the "bond system", and this includes the contacts between grains, microcracks, etc. (*e.g.*, [46-49]).

An analogue for the soft-hard system is well known for liquids with bubbles where the maximum nonlinearity is observed for a gas volume fraction of less than 10^{-3} (*e.g.*, [7]). Under such conditions, the average density of the medium is only slightly affected by

([2]) Hence, the measured strain is due to the deformation of the soft bond system. Because hard portions of the system prevail in size, the measured bulk strain it is an underestimate of the local strain by at least two orders of magnitude. This is an important and often overlooked consideration.

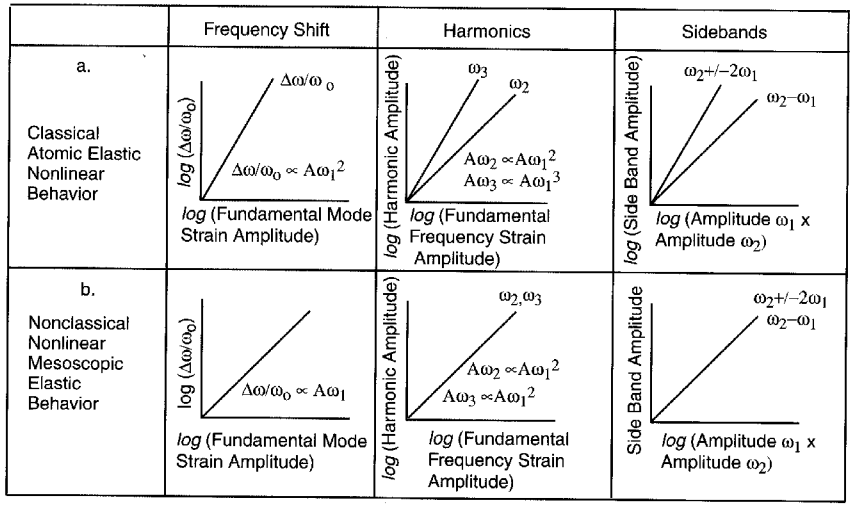

Fig. 21. – Comparison of strain dependences for frequency shift, harmonics and sidebands for a classical model (a), and for a hysteretic model (b). $\Delta\omega = \omega - \omega_0$, where ω_0 is the fundamental frequency, $A\omega_1$ is the fundamental amplitude from the Fourier transform of the time series signal, $A\omega_2$ is the amplitude of the second harmonic, and $A\omega_3$ is the amplitude of the third harmonic.

the presence of bubbles. At the same time, the pressure in the gas phase dramatically affects the compressibility of the gas-liquid mixture and especially the dependence of the sound speed on the pressure, which characterizes the nonlinear response of the medium. A similar behaviour is demonstrated by waterlike porous media in which the shear modulus is small compared with the bulk modulus (*i.e.*, the shear wave velocity is much smaller than that of longitudinal waves) (*e.g.*, [7]). In such cases the parameter of nonlinearity β may reach values of 10^4–10^5, as compared to 1 to 10 for "classical" gases, liquids and solids.

In the following discussion, let us test several simple physical models in order to see if they may provide some insight into the mechanism of nonlinear response.

4·1. *Hertzian contacts.* – A starting point model of nonlinearity in rock can be based on representing the rock as a system of dry, contacting grains as shown in fig. 22. These contacts are much softer than the matrix material, the grains themselves, and therefore play the primary role in the nonlinear elastic response of the medium. In this model, the distance change Δ between the grain centres is related to the compressing force F by the Hertzian contact law (*e.g.*, [41]),

$$\Delta = \left(\frac{3(1-\nu^2)F}{4ER^{1/2}}\right)^{2/3}, \tag{11}$$

where E is Young's modulus of the material, ν is Poisson's ratio, and R is the grain radius.

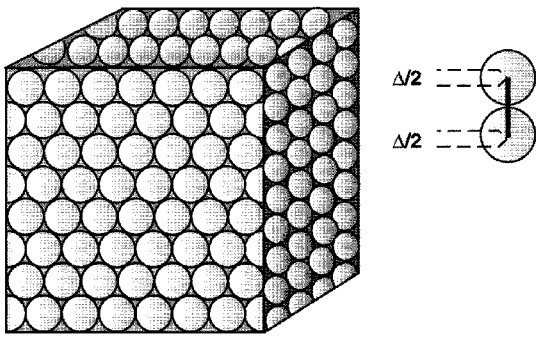

Fig. 22. – An aggregate of contacting grains.

For a dry medium composed of spheres, this model yields the following one-dimensional EOS relation [47]:

$$\sigma_{\text{eff}}(\epsilon) = \frac{\bar{n}\,(1-q)E}{3\pi\,(1-\nu^2)}\epsilon^{3/2}, \tag{12}$$

where σ_{eff} is effective stress, $\bar{n}$ is the average number of contacts per grain and q is the fraction of empty (porous) space per unit volume. For a random packing of nonconsolidated grains, $\bar{n} = 8.84$ and $q = 0.392$ [50]. It is evident that the contact contribution to the sound speed, $c = (\rho^{-1}\mathrm{d}\sigma_{\text{eff}}/\mathrm{d}\epsilon)^{1/2} \propto \sqrt{\epsilon}$, tends to zero at small positive strains (negative strain means that grains separate, and no contact forces are present). However, $\mathrm{d}c/\mathrm{d}\epsilon$, which is one measure of nonlinearity, tends toward infinity! In real experiments the aggregate is subject to a static pressure creating a constant prestrain ϵ_0, and for small one-dimensional perturbations, we can expand c into the series (3), where the modulus is

$$M = \frac{\bar{n}\,(1-q)E}{2\pi\,(1-\nu^2)}\epsilon_0^{1/2}, \tag{13}$$

and the quadratic and cubic nonlinearity coefficients are

$$\beta = 1/2\epsilon_0\,, \quad \delta = 1/6\epsilon_0^2. \tag{14}$$

In rock the role of prestrain can be played by a hard, consolidated portion of contacts and/or by the pressure from the upper layers of the earth.

Some interesting properties of granular materials follow from these simple results. For instance, the nonlinearity parameters do not depend on grain size or on their composition, but on prestrain ε_0, *i.e.*, on static pressure. These results were confirmed in experiments with lead shot and tuff excited at frequencies of few kilohertz by a vibrating table [46]. The values of ϵ_0 were controlled by loading masses. From measurements of second and third harmonics, both formulae (14) agreed with the experiment; the parameter β exceeded 10^3 and δ the values of 5×10^6.

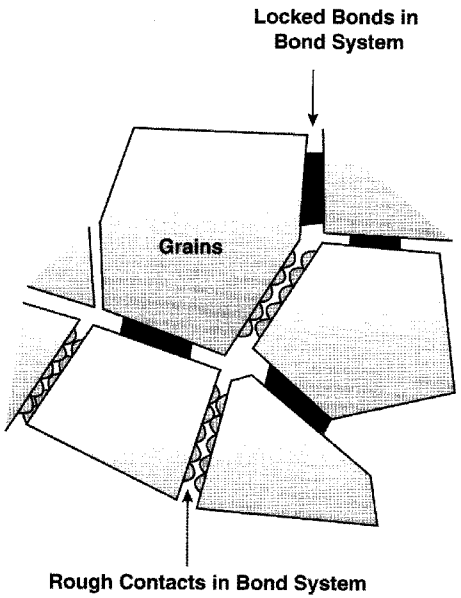

Fig. 23. – Granular medium with rough contacts.

Hence, this model predicts a very strong nonlinearity due to the contacts as compared with the solid matrix, and it admits many effective extensions. One of them deals with small-scale multicontact interfaces between larger grains, yielding a significant local amplification of nonlinearity from local stress concentrations. There is significant evidence that the stress path in rocks may not be homogeneous (*e.g.*, [1]). Preliminary estimates [49] show that, for larger grains (of radius R) in contact with smaller hemispheres of radius r (fig. 23), the nonlinear portion of the EOS (12) and, correspondingly, nonlinearity parameters (14) acquire an additional term of $s(R/r)^{3/2}$, where s is the relative contact area occupied by small-sphere contacts (the remaining area is assumed to be cemented). This approach (see also [51]) can be extended to more complicated fractal structures. Note that in [48] experiments similar to those in [46] were described but with larger and larger grains which were not exactly spherical and had different sizes. In this case, nonlinearity was even stronger, and for the third harmonic, a nonclassical, approximately quadratic dependence on the excitation amplitude has been observed. This may shed some light on the role of nonconsolidated components in mechanisms of nonclassical elasticity.

4·2. *"Bed of nails" model of cracks.* – Another important element of rock structure are microcracks. The fact that cracks strongly enhance nonlinearity has been experimentally confirmed numerous times for different materials, including ice [52]. Opening and closing of cracks can radically change the elastic modulus.

A corresponding extension of the Hertzian model (that is similar to the "bed of nails" model introduced by Walsh [53] for the linear problem but is based on contact nonlinearity) was considered by Nazarov and Sutin [54]. In this model, portions of the bond system are assumed to be rough, and, under compression, they randomly contact each other (similarly to fig. 23). The force on individual contacts depends on the shape of the contacting surfaces. In order to understand the effects of contact geometry on the result, three shapes were considered: spheres (as above), cones, and wedges. The force is proportional to $\epsilon^{3/2}$, ϵ^2, and ϵ, for the spheres, cones, and wedges, respectively. A distribution function $W(h)$ of contacts within a single crack is proportional to $\exp[-h/h_s]/h_s$, where h is the height of the contact and h_s is a constant.

The quadratic nonlinearity parameter is found to be

$$2\beta = \frac{bN_c}{7\,(1+3aN_c/5)^2}, \tag{15}$$

where

$$\begin{aligned} a &= \pi R^2 h_s\,(E/\sigma_0)\,(1+h_s/d_0)^{-1}\,, \\ b &= \pi R^2 h_s\,(E/\sigma_0)^2\,(1+h_s/d_0)^{-3}\,. \end{aligned} \tag{16}$$

Here σ_0 is a static stress, d_0 is the average distance between the crack surfaces, E is Young's modulus of the material, and N_c is the unit volume number of cracks. The authors estimate that for cracks with conical contacts reduce the effective linear parameters of the medium, Young's modulus and Poisson's ratio, by only about 1%, but increase the quadratic nonlinearity parameter β up to a value of 500.

Note that acoustical remote sensing methods have been suggested for nonlinear crack diagnostics (*e.g.*, [55]) *in situ*, however, their feasibility has not been tested.

4·3. *The role of fluids in the bond system.* – It is common knowledge that the presence of fluids significantly affects linear properties of rocks (sound speed, losses), see *e.g.*, [56], [57] and [58]. These effects are often considered in the framework of the phenomenological Biot theory which provides at best a qualitative description. The experiments mentioned above [22] show that the elastic nonlinearity of rock is also significanly affected by the presence of fluid.

Let us briefly discuss nonlinear models based on wet Hertzian contacts. A simplest case is that of a 100% filling of the intergrain space (100% saturation) [47]. In this case, the fluid provides an additional elasticity effect to that of grain contacts. The resulting EOS (neglecting the atomic fluid nonlinearity) has the form

$$\sigma_{\rm eff} = \frac{K_f}{\phi + (1-\phi)K_f/K_s}\epsilon + \frac{\overline{n}(1-\phi)E_s}{3\pi(1-\nu_s^2)}\epsilon^{3/2}, \tag{17}$$

where K_f and K_s are the bulk modulus of the fluid and solid phase, respectively, and ϕ is the porosity.

Relation (17) predicts a decrease in nonlinearity of the entire medium, but it applies only near 100% fluid saturation. This is understandable: complete pore filling adds to the rigidity of the system. However, for a relatively small degree of saturation the effect can be the opposite because strong effects such as capillary and dipole forces enter in. Indeed, the observations mentioned in fig. 8 indicate that for small and moderate water saturation the nonlinearity *increases*. To describe this effect it seems necessary to consider forces acting on grains due to a thin fluid film between them. For instance,

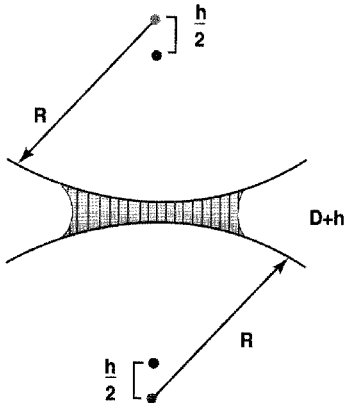

Fig. 24. – Hertzian contact containing water.

these forces were considered in detail from the thermodynamic viewpoint by Tutuncu and Sharma [58] and their predictions provide reasonable agreement with measurements of sound velocity and attenuation.

For nonlinear effects, we applied a more simple and direct consideration [49] of the contact between two spheres of equal radii R (fig. 24) divided by a thin water layer. The attractive capillary force between them is

$$F_c = \frac{2V\gamma\cos\Theta}{(D+h)^2}, \tag{18a}$$

where γ is the surface tension coefficient, Θ is the angle between surfaces of fluid and solid, V is the volume of fluid between contacting grains, D is the minimal equilibrium thickness, and h is the displacement due to external (acoustic) stress. Considering the change of the latter parameters due to acoustic deformation at a fixed fluid volume and averaging the material over the bulk, it is possible to find the contribution of capillary forces to the EOS:

$$\sigma_c = \frac{2V\gamma\cos\Theta}{\pi R^2 D^2\,(1+2\varepsilon R/D)}. \tag{18b}$$

This stress must be added to the Hertzian stress considered above. It follows from here that the intergrain fluid decreases the linear elastic modulus and for a harmonic strain this effect increases with growth of the strain amplitude (*i.e.* the cubic nonlinearity coefficient is negative). These results qualitatively agree with experiment where the resonance frequency decreases with the excitation amplitude. Note that analogous results were obtained by Nazarov [59] for fluid-filled cracks with planar geometry.

Preliminary estimates show that an especially strong fluid contribution should be expected when grain contacts are separated with very thin fluid layers, of the order of few or few tens of monolayers. In this case, a dipole van der Waals force can be dominant.

For a flat contact, this force is

$$F_d = \frac{\bar{A}}{6\pi d_0^3}, \tag{19}$$

where d_0 is the thickness of the gap, and $\bar{A}$ is the Hamaker constant (of order 10^{-13}–10^{-14} erg for water). The corresponding stress should again be added to the Hertzian force. It should be noted that elasticity of fluid films can be hysteretic (due to different values of Θ for the oscillating displacements (18a) [60]) and also provide the time-logarithmic relaxation of parameters as demonstrated in [24]. This is an area of intense study.

A significant study based on the theory of liquid-vapour balance developed in [61] was performed by Van Den Abeele *et al.* [22]. Their estimates indicate that the influence of fluid can be strong for pore sizes of the order of or less than a micron. They also interpreted the macroscopic effect of a small amount of water by a shifting of hysteretic elements in PM space discussed above.

4·4. *The role of transverse deformations.* – In a series of papers by D. Johnson and colleagues (*e.g.*, [62]), a detailed analysis of nonlinear properies of granular media under the influence of static pressure was carried out. These authors took into account Hertz theory and the Mindlin relation (and its variations) stating that, upon normal compression, a tangential displacement, s, may arise at contacts that, in general, creates an additional transverse force:

$$F_\tau = \frac{4\mu a(\Delta)s}{1-\nu}. \tag{20}$$

Here again, Δ is the relative displacement of spheres, μ is the shear modulus of the material, and a is a characteristic length depending on the nature of surface contacts. For a "pure" Hertzian contact with reversible slip, $a = 0$, but for a rough, nonslip contact, it is $\sqrt{R\Delta}$ or, in case of precompression with an initial contact radius b, $[(R^2\Delta^2 + b^2/4)^{1/2} + b^2/2]^{\frac{1}{2}}$. This results in some new features such as the dependence of forces and energy on path of deformation. Indeed, in general, transposing of normal and transverse displacements changes the work of the external force. This is actually a hysteretic phenomenon, that causes, *e.g.*, attenuation of an elliptically polarized acoustic wave. However, a possible role of this mechanism in rock hysteresis is still unclear. See [62] for more.

4·5. *Granato-Lücke model.* – In many hysteretic materials, the bond system is crystalline. Therefore dislocations within the crystalline lattice of the bond system could conceivably produce the nonlinear response. A physical model based on dislocations in metals was suggested by Granato and Lücke (GL) as early as in 1956 (see [5]). They used an analogy between a segment of a dislocation line pinned to impurity atoms, and the motion of a string in order to describe elastic deformations (fig. 25a). As the stress increases (normally shear stress), dislocations deform like pieces of string until, at some critical stress, they are disconnected from all impurity atoms between the nodes of a crystalline structure. As a result, the material becomes softer, which results in strong nonlinearity in the stress-strain dependence (fig. 25b, solid line)). This process is irreversible at the atomic scale: upon reducing stress, the system returns to equilibrium along a "soft" line. However, the resulting equilibrium state may be the same before and after inducing the dislocations to react. The model also incorporates slow dynamics, because the equilibrium state takes some time to restore. In reality, the distances

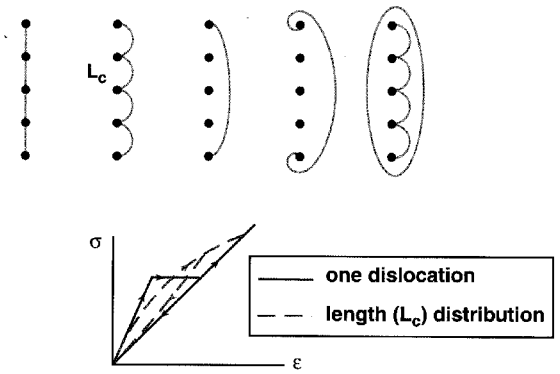

Fig. 25. – (a) Granato-Lücke model of string-like dislocations. (b) Resulting stress-strain curve for a single dislocation (solid line) and a distribution of dislocations (dashed line).

between the sticking points are statistically distributed, which smooths the hysteretic loop (fig. 25b, dashed line). Hybrids of the GL model include other aspects such as frequency dependence. In spite of some disadvantages, this model was truly a pioneering micromodel for hysteretic dynamic behaviour.

If we consider a triangular stress-strain curve (fig. 25b) with a given strain ϵ_1 of depinning for each element (string), and the initial line $\sigma = A\epsilon$ (at $\epsilon < \epsilon_1$) is sufficiently close to the line $\sigma = A_0\epsilon$ after depinning (weak nonlinearity), then on the plane of $\epsilon - \epsilon_1$, $\sigma - A_0\epsilon$ we have almost a rectangular-triangle loop. This is similar to the PM space model considered above. Indeed, if we have a distribution of these elements in values of ϵ_1 (or A) which is a constant for a narrow range of ϵ_1 and zero outside of it, we obtain the same scalings as for the PM space model (rectangular triangles instead of rectangles). This implies that the HEUs in the PM space model may be qualitatively analogous to the GL dislocations, where the contacts between grains have tangential deformations (see Asano's "ratchet" model mentioned above).

4·6. *Slow dynamics.* – As mentioned in the experimental portion of this paper, hysteretic nonlinearity typically is accompanied by slow dynamics, slow recovery of the initial equilibrium state after a disturbance. Earlier models of relaxation in rock were based on a phenomenological description. A simple model for the nonlinear portion of the elastic modulus, ΔK, assumes a constant relaxation time τ (or several time constants) [64],

$$\tau \frac{\mathrm{d}\Delta K}{\mathrm{d}t} + \Delta K = \lambda G^n . \tag{21}$$

When, at $t = 0$ and $\Delta K = 0$, a constant-amplitude signal having the form $G\theta(t)$ is introduced into a material, where $\theta(t)$ is a step-function (Heaviside function) equal to 1 for $t > 0$ and 0 for $t < 0$, this equation gives

$$\Delta K(t) = -\lambda G^n \left(1 - e^{-t/\tau}\right). \tag{22}$$

However, in all experiments in rock and related materials that we are aware of [24,25] the relaxation process is *logarithmic* in time rather than exponential. Tencate *et al.* [24] proposed a possible physical model for this effect based on the statistics of bond restoration at microcontacts in granular media after their rupture by an acoustic disturbance. The rate of this process, $g(\mathcal{E})$, is proportional to $\exp[-\mathcal{E}/kT]$, where $\mathcal{E}$ is the corresponding energy barrier, k is Boltzmann's constant, and T is the temperature. In turn, the density $\rho(\mathcal{E})$ of unrecovered bonds is proportional to $\exp[-g(\mathcal{E})t]$. The elastic modulus, K, is assumed proportional to the total contact area between grains. Thus, the unrecovered part of K is proportional to $\int_{\mathcal{E}_1}^{\mathcal{E}_2} \rho(\mathcal{E})\mathrm{d}\mathcal{E}$, where $\mathcal{E}_1 < \mathcal{E} < \mathcal{E}_2$ is the interval of barrier energies participating in the process. If the range of $\mathcal{E}_2 - \mathcal{E}_1$ is reasonably small, it can be presumed that $\rho(t = 0) \approx \rho_0(\mathcal{E}_c)$ and $\mathcal{E}_c$ is a characteristic energy within this interval, so that only variation of the exponents is taken into account. As a result, for the time variation of the modulus, the logarithmic relation readily follows:

$$K(t_2) - K(t_1) \sim \ln(t_2/t_1). \tag{23}$$

The time interval in which this formula applies is limited by the above assumption that $\mathcal{E}_c$ lies in the barrier energy range. The authors estimate $\mathcal{E}_c \sim 1$ eV and conclude that the model works for crystal defects, some dislocations, or surfactant bonds. To explain experimental data, they also infer that, apart from the acoustic strain, thermal activation softens the bonds. This work can be important for understanding the mechanisms and scale of hysteretic nonlinearity.

A recent experimental and theoretical study by Josserand and colleagues [66] of memory effects in vibration-induced compaction of granular materials describes some intriguing similarities to granular solids. Josserand and colleagues monitor the grain packing *vs.* exitation by tapping. This is analagous to the "conditioning" portion of experiments conducted in rock (for instance those shown in fig. 9). Interestingly, the evolution of the packing fraction of the grains is dependent on the future evolution of the packing fraction and on the previous disturbance history. This is a memory effect during conditioning, and may be related to "discrete memory" as we know it. The "recovery" of the material after the disturbance is complete is not monitored in this study. This could be an interesting experiment to see whether or not recovery has a log(time) dependence as it does in rock.

5. – Nonlinear waves in rocks

To explain experimental data, it is necessary, along with the construction of material models, to understand the peculiarities of waves in these materials. From the above considerations and experimental data it can be expected that these processes are more complex than those in nonlinear acoustics describing most fluids and intact solids.

For the wave models that follow, we begin with the basic classical equation (2) in which only physical nonlinearity is taken into account([3]). In each case, we introduce nonclassical descriptions after the classical descriptions.

5·1. *Travelling waves.* – We begin by considering travelling (progressive) waves in an unbounded material with strong nonlinearity. For a one-dimensional travelling wave, the

([3]) As noted, this equation is sufficient for the description of waves in both Lagrangian and Eulerian coordinates, provided the dependence $\sigma(\epsilon)$ is known and physical nonlinearity is strong. This reduces the total order of governing equations and simplifies the description.

strain $\epsilon \approx -v/c$, where $v = u_t$ is the particle velocity, and c is the sound velocity([4]). When the Taylor expansion (5) for c is valid, a well-known solution in the form of a simple (Riemann) wave follows from eq. (2):

$$\epsilon = \psi\left[x - c(\epsilon)t\right], \tag{24}$$

where ψ is an arbitrary function defined by the initial condition, and $c(\epsilon)$ is the local wave speed. Propagation of such a wave in acoustics is known to result in the appearance of shocks and then formation of sawtooth (see fig. 1) or of triangular waves (*e.g.*, [7]), which dissipate as x^{-1} or $x^{-1/2}$, respectively. Using only the quadratic approximation, harmonic amplitudes of the initially sinusoidal wave are defined (before shock formation) by the well-known Bessel-Fubini expansion in which all harmonics are expressed in terms of Bessel functions. For moderate distances (much less than that required for shock formation), the second-harmonic amplitude is proportional to the distance x, and the third-harmonic one is proportional to x^2. The quadratic nonlinearity parameter, β, can be experimentally obtained from a measurement of the amplitude of the second harmonic of displacement, A_2, generated at a distance x from a pure tone (single frequency) source signal,

$$\beta = \frac{8A_2c_0^2}{A_1^2\omega^2 x}, \tag{25}$$

where ω is the fundamental frequency and A_1 is the amplitude at the fundamental frequency. In rocks and other materials, higher-order terms are used in order to describe the nonlinear response. For instance, the third-harmonic amplitude is proportional to ${A_1}^3$; its value depends, in general, on both quadratic, β, and cubic, δ, nonlinear parameters. More details can be found in [65].

5·2. *Travelling waves and hysteresis.* – Looking back at the primary indicators of nonlinear structural elasticity described earlier, we saw that nonclassical, hysteretic behaviour is characterstic. Thus we turn to wave solutions that can describe this behaviour.

The evolution of a nonlinear wave in hysteretic media described by eq. (6) is considerably different from that of a wave in atomic elastic media. Several problems of this kind have already been addressed in [67-70, 72]. First, note that for two basic hysteretic models shown above in fig. 18, "ratchet" and "slider" types, the wave distortion processes are significantly different. In refs. [68] and [70] the hysteretic relation of type (6) has been considered in the case when the "classical" parameters β and δ are absent and the nonlinearity is of a "ratchet" type (fig. 26a): σ and ϵ go to zero simultaneously. In this case shocks do not appear. However, due to the singularity at the wave maximum, the portions of the wave on either side of the wave peak move with different velocities, thus "consuming" each other and resulting in the formation of a triangular profile without shocks. The corresponding qualitative pattern of the evolution of the pulse is shown in fig. 26b taken from [70]. When the wave reaches the triangular stage, the amplitude ϵ_m of an initially sinusoidal wave nonlinearly attenuates as $1/x$, and is proportional to

([4]) Indeed, $\epsilon = \partial u/\partial x$ and $v = \partial u/\partial t$. For small nonlinearity (even if it is much stronger than that in "atomic" materials), in a travelling wave $\partial u/\partial t \approx -c(\partial u/\partial x)$, and therefore, $\epsilon \approx -v/c$. In this sense, the strain plays the role of the acoustic Mach number. Although we consider nonlinear effects, this relation is valid in the first approximation.

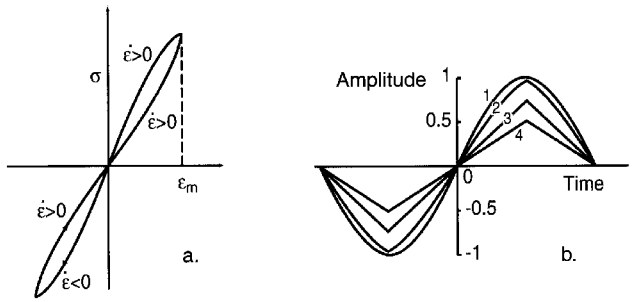

Fig. 26. – Propagation of a unipolar pulse in a medium with hysteretic nonlinearity. (a) Stress-strain relation. (b) Perturbation profiles with progressive distance (1-4). Phase $\theta = \omega t$, and θ_m is the duration of the perturbation.

$\sqrt{\epsilon_0}$ where ϵ_0 is the initial wave amplitude, as shown in [72]. In the latter work, the "slider" model is considered when, for a periodic process, EOS is a loop going around the center so that $\epsilon \neq 0$ when $\sigma = 0$. In this case, ϵ_m is again proportional to $1/x$ but asymptotically so, and it does not depend on ϵ_0 (similar to the case of a sawtooth wave in a nonhysteretic medium with quadratic nonlinearity). Note that in the general case, when classical nonlinearity is present along with the hysteretic one, the wave can contain both "triangles" and shocks.

5·3. *Standing waves in resonators.* – The theory for standing waves is more complicated due to nonlinear interactions of oppositely propagating waves. In the general case, one should solve a nonlinear wave equation (2) with an external forcing and boundary conditions at the end of the bar. In terms of displacement, u, this equation is

$$\rho\left(\ddot{u} + \frac{1}{\tau_0}\dot{u}\right) = \frac{\partial\sigma(x)}{\partial x} + \frac{1}{2}F_0(x)\left[e^{i(\omega+\Delta\omega)t} + \text{c.c.}\right], \tag{26}$$

where $F_0(x)$ is the external force amplitude, $\Delta\omega$ is the frequency shift (detuning) from a linear resonance mode, and τ_0 is a characteristic time of linear damping: $\tau_0 = Q_n/\omega_n$, Q_n being a linear quality factor at a resonance frequency ω_n.

For small nonlinearity, the structure of resonance modes is close to that of the linear system although their amplitudes are strongly affected by nonlinear interaction. Thus, it is adequate to use an expansion of the solution for u into the modal series:

$$u = n\sum A_n(t)\Phi_n(x), \tag{27}$$

where Φ is the eigenfunction of the linear wave to be found with the use of corresponding boundary conditions at the bar ends (For a bar of the length L with free ends, $\Phi_n = \cos kx$, where $k = n\pi/L$ and n is an integer mode number.) As a result, a system of ordinary differential equations for A_n follows, that can usually be reduced to a system of a few interacting resonant modes (*e.g.*, [6]).

The efficiency of nonlinear response depends on the boundary conditions at the bar ends. For the free ends, third harmonic amplitudes will be cumulatively generated,

unlike the second harmonic. This may result in domination of the third harmonics in the experiments, even if the quadratic nonlinearity of the material is large as it often is, especially for longitudinal waves in atomic elastic media. The explanation is as follows. If the bar ends are fixed (*e.g.*, due to loading by heavy masses), the wave pressure is reflected in-phase, and (in a nondispersive material) the harmonics will continue to accumulate upon end reflections as in a travelling wave. In other words, all standing modes will be generated in phase. However, for the free ends typically used in such experiments, the pressure phase change is 180 degrees upon reflection. As a result, the fundamental (first) and third harmonics will be shifted, respectively, by π and 3π whereas the second harmonic by 2π (as the square of the first one), and it will be generated with the opposite phase with respect to the primary wave, thus decreasing and suppressing the existing second-harmonic field due to interference. The wave at frequency 2ω (and all even harmonics) will alternately grow and decay upon reflections so that the effect is not cumulative (*e.g.*, [6,7]). On the other hand, the third harmonic remains in phase with the first one (their relative shift is 2π) and shows progressive amplitude increase independent of whether the boundary is fixed or free.

Substituting into (26) a solution of the form (27) for the n-th mode, *e.g.*, $u = U\cos k_n x \exp[-i(\omega_n + \Delta)t/2]$, multiplying by $\cos k_n x$ and integrating over the length L of the bar, we obtain an equation for the amplitude U in equilibrium,

$$\rho\left(-\omega_n\Delta + i\omega_n/2\tau_0\right)U = k_n\left\langle\sigma_1^N(|U|)\right\rangle + \langle F_{0n}\rangle\,. \tag{28}$$

Here the stress is $\sigma = E(\partial u/\partial x) + \sigma^N(\epsilon)$ with N denoting the small nonlinear portion, σ_1^N is the first temporal harmonic of nonlinear stress, and $\langle f\rangle = L^{-1}\int_0^L f(x)\cos k_n x\mathrm{d}x$ denotes spatial averaging of the corresponding value f, and E is the Young modulus, so that $c_0 = \omega_n/k_n = (E/\rho)^{1/2}$. Hence, we have an equation for the amplitude-frequency resonance dependence, $|U|(\Delta)$,

$$|U| = \frac{\langle F_0\rangle/2\rho}{\sqrt{\left(2\Delta\omega_n + k_n\left\langle\sigma_1^N\left(|U|\right)\right\rangle/\rho|U|\right)^2 + (\omega_n/2\tau_0)^2}}. \tag{29}$$

The result clearly depends on the EOS of the medium. In a classical cubic medium, when $\sigma^N \propto u^3$, this relation defines a well-known nonlinear resonance curve with the nonlinear frequency shift proportional to $|U|^2$. In hysteretic media, $\left\langle\sigma_1^N\left(|U|\right)\right\rangle \propto |U|$, and the frequency shift is also proportional to $|U|$.

To find a higher, m-th harmonic of, say, the first-mode oscillations, one should use a perturbation method. That is, after obtaining the basic amplitude as above, we represent a solution in the form $u = u_1 + u_m$, where $u_1$is the above solution at the fundamental frequency and $u_m = U_m\cos k_m x\exp\left[im(\omega+\Delta)t\right]$ corresponds to the harmonics possibly resonating at a higher (m-th) mode. As a result, the equation for U_m has the form (28) where now the corresponding m-th harmonic of $\sigma_m^N(|U|)$ should be taken. Thus, we get an expression for $U_m(\Delta)$ that is similar to (29) in which the role of the force $\langle F_0\rangle$ is played by the first harmonic of stress, $k_n\left\langle\sigma_1^N\left(|U|\right)\right\rangle$. For classical nonlinearity, the amplitude of the second harmonic in resonance is proportional to $|U|^2$, and for the third harmonic, to $|U|^3$. For nonanalytical, hysteretic models we obtain different dependences which are often observed in experiments with rocks.

For hysteretic media, the interaction of counterpropagating waves reflected from the bar ends is associated with a complex picture of switchings corresponding to nonanalytical

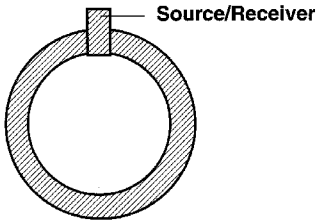

Fig. 27. – Ring resonator.

points in the EOS. For small distortions of initially harmonic waves, spectral expansion is typically used to find the small higher harmonics [67,71]. Van Den Abeele and Tencate [73] applied a similar approach to the average elastic modulus found from the PM space model.

Another model that is valid for strong deformations of the wave profile [72] is a ring resonator (similar to that used in experiments described in [6]) where a resonance mode can be a wave travelling around the ring and undergoing nonlinear distortions until it is balanced with a harmonic source applied at some point (fig. 27). A hysteretic medium described by the two aforementioned types of phenomenological stress-strain loops has been considered in [72]. In the "ratchet" case, the strain amplitude in a steady-state regime, ϵ_m, is proportional to $\sqrt{u_0}$, where u_0 is the excitation amplitude, and the effective Q-factor of the resonator is proportional to $1/\sqrt{u_0}$ that is similar to nonlinear oscillations in a resonator with a "classical" quadratic medium [7]. For a "slider"-type hysteresis, $\epsilon_m \propto u_0$ and Q is independent of amplitude, just as in a linear medium! However, in this case the wave form is still nonlinear, as shown in fig. 26b, and in case of free damping, its amplitude will, at a nonlinear stage, attenuate at a power rate, not exponentially.

All these results are valid when the hysteretic loop consists of parabolic sections (an analog of quadratic nonlinearity). Otherwise, a frequency shift occurs, which can be proportional to $|u_0|$, which is impossible for an analytical stress-strain dependence but is observed in experiments.

5·4. *Numerical simulations.* – For media with hysteretic properties, analytical solutions are rare, and numerical experiments are necessary. The difficulty associated with the discontinuous stress-strain dependence was addressed by using its discrete Fourier series expansion([5]). Strong wave distortion was calculated by a finite-difference procedure. Frequency-dependent attenuation was accounted for at each step in the iteration by a commonly applied *ad hoc* method where dissipation is proportional to velocity. See also, for instance, the work of Day and Minster [74].

Recently, Delsanto and others [75] applied the "local interaction simulation approach" (LISA) to numerical model resonance and pulse-mode waves in one dimension, based on implemenation of the PM space model. Figure 28 shows model predictions from LISA for a quasistatic (a) and (b)-(d) for dynamical numerical experiments. An important

([5]) An analytical expression describing the distortion of a pulsed signal was then obtained; however, this expression was found using perturbation theory, so that it is restricted to small distances from the source.

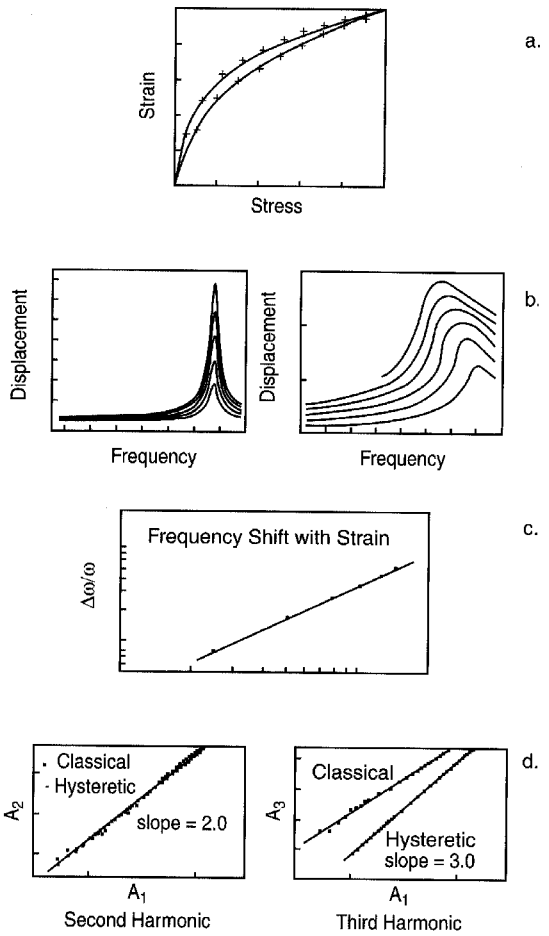

Fig. 28. – Numerical results obtained from LISA, by implementing the PM space model. A PM space similar to that deduced from laboratory quasi-static results by Guyer *et al.* [14] was used. (a) Quasi-static stress-strain response. (b) Resonance curves for successively increasing amplitudes in an classical (atomic elastic) material (left) and nonclassical (highly nonlinear) material (right). (c) Predicted dependence of frequency shift on strain showing the correct slope of 1. (d) Second (left) and third harmonics (right) as a function of strain amplitude, for classical and nonclassical materials.

feature of LISA is that it provides the capability of implementing at the local level very complex mechanisms. In fact, the method allows full freedom in the choice of interaction between nodes, representing the material cells. It is also possible, by splitting the nodes at the interfaces between different material components, to consider problems of interface delaminations and other surface flaws. One can also assume that the local elastic forces

may undergo local variations, in particular nonlinear ones, such as leading to hysteretic or plastic behaviour. This will be important as the mechanism of nonlinearity is unravelled. This group is in the process of implementing slow dynamics and expanding the model to two- and three-dimensional predictions.

6. – Field experiments

Field observations of nonlinear effects have a relatively long history. *In situ* experiments include studies using both active and passive source observations. Some of early experiments are described in a special issue of *Physics of the Earth and Planetary Interior*, No. 1 (1988). Results include field observations from earthquakes, earth tides, and vibroseismic sources. However, these experiments are often difficult to interpret and therefore the results are of uncertain reliability. Indeed, considering the complexities of the near surface of the earth and the distortions it imposes on seismic waveforms, both linear and nonlinear, it is extremely difficult to extract and analyze the nonlinear response *in situ*. Here we present a selection of some observations.

6·1. *Active observations.* – Observations in the field using large vibrator sources have been made by several groups, including Beresnev and Nikolaev [76] at the Institute of Earth Physics in Moscow, and the group at Los Alamos in collaboration with researchers at Lawrence Berkeley Laboratory (T. V. McEvilly, private communication, 1994). These observations have involved standard seismic exploration sources (such as vibroseis) and detectors. Based on our experience, the results of these experiments have been ambiguous, due to the possibility that the observed harmonics could be attributed to the nonlinearity of the sources (seismic vibrators are notoriously nonlinear). Observations by Beresnev and Nikolaev seem to indicate that nonlinear response was developed along the propagation path in similar studies. However, these results were still disputed in some publications arguing that the observations could be attributable to the source.

Nikolaev and co-authors [77,78] performed field experiments in which the response of a vibrator resulted in time-average elevation of near-source ground area. According the nonlinear wave theory, this effect is a result of a quadratic nonlinearity in the medium.

Note that at times field observations have been interpreted in a more unconventional manner. For example, in papers [92] the possibility was discussed of wave amplification via "dilatons" defined as "short-lived microdynamical density fluctuations" which are able to lock-in energy from the surrounding medium and, after exceeding some threshold, release it as an elastic wave. In principle such processes are possible in thermodynamically nonequilibrium states but no detailed development of this hypothesis has been done, and no direct experimental evidence of such mechanisms in rocks exist.

6·2. *Earth tides and nonlinear response.* – A pioneering work in the study of the nonlinear response of the whole earth to the tides caused by lunar and solar motions was reported, for example, in [79,80]. Study of earth tides for nonlinear response has several advantages over the use of long-period seismic waves; earth tides are narrow band, and tidal forces are precisely known from astronomy. A disadvantage in the use of earth tides is contamination by ocean tides and their nonlinear influence, and poor spatial resolution because the wavelengths are so long and maximum strains are of order 10^{-8} [79].

The careful study presented by Agnew [79] is a good example. He hypothesized that the primary nonlinear effects come from the nonlinear EOS curve and hysteresis. Data from a three-component laser strain meter located at Pinon Flats Observatory in

southern California were used in the analysis. Data collected for 5.7 years were used from which Agnew averaged spectral portions 100 days each in duration. From his analysis the harmonics of tidal frequency were retrieved. Agnew found that the third harmonic (M6) prevailed over the second harmonic (M4), which is an indicator of nonclassical behaviour.

6·3. *Strong ground motion.* – An obvious candidate for the study of nonlinear effects are strong earthquakes, and this has become a huge topic within itself, especially in the last five years (*e.g.*, [84, 28]). The bulk of papers on this topic, known as *strong ground motion*, can be found in the *Bulletin of the Seismological Society of America*. A critical aspect of strong ground motion is the presence of consolidated or loosely consolidated sedimentary layers at the Earth's surface (see, *e.g.*, [83]). It is well known that the resonance wave amplification can typically be several times larger than that for a nearby rock site assumed to have the identical source and wave path effects. This amplification leads to larger strain levels which may induce, or further enhance, nonlinear response, such as the nonlinear resonance frequency shift in the low-sound speed upper layer and losses due to material softening and hysteresis. Examples of this behaviour include all of the most damaging earthquakes of the latest decade, including the 1985 Michoacan (Mexico), the 1989 Loma Prieta (California), the 1994 Northridge (California), and the 1995 Kobe (Japan) earthquakes. Typical detected wave strains in these earthquakes are 10^{-4} to 10^{-9} in frequency range from 0.1 to 100 Hz. The analysis of Field and colleagues on the 1994 Northridge earthquake presented the first of convincing observations of nonlinear behaviour in sediments from an earthquake source [85].

7. – Potential applications

We believe that potential applications of monitoring nonlinear response exist in both geophysics, seismic hazards, material science and nondestructive testing (NDT). Geophysical applications are only beginning to be realized. Realistically, applications such as monitoring of physical property change, both in the laboratory and in the field, are areas that are now being addressed. All our collaborators are active in these areas. In particular, we anticipate that potential borehole and core applications may well come about. For example, extraction of nonlinear parameters from borehole or core methods that could be applied to rock strength issues such as borehole stability and hydraulic fracturing may be quite realistic. Application of these methods may also make it possible to localize regions of macro- and micro-crack appearance in the vicinity of structures that are of high potential risk, such as nuclear power stations, chemical installations, dams, etc., in active earthquake regions. Other potential applications are remote monitoring of areas in the Earth's crust that may undergo stress changes using passive or active seismic monitoring, as well as petroleum exploration, although additional study is needed to evaluate their feasibility. Nonlinear methods of evaluation of sea sediments [86] are also promising.

7·1. *Nondestructive testing of materials.* – In recent works by several groups, applications of nonlinear response to nondestructive testing (NDT) of materials has proven to be a powerful tool in interrogating materials for damage, and the area is expanding rapidly. The original work in this area can be attributed to the group at Nizhny Novgorod (*e.g.*, [21, 87]). Some work has been done in study of progressive fatigue damage in rock and concrete [90, 88], but the bulk of studies have been in other materials that exhibit the same manifestations of nonlinear response as rocks, see, *e.g.*, [1, 89, 90, 25].

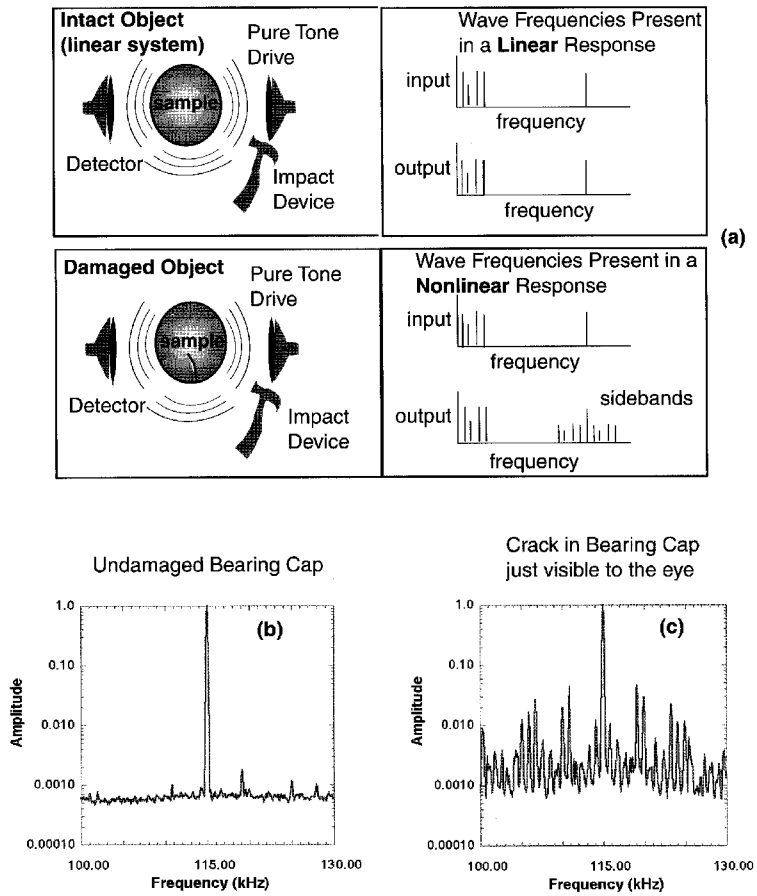

Fig. 29. – Nonlinear Wave Modulation Spectroscopy (NWMS). (a) Experiment, (b) Spectrum of response in undamaged sample. (c) Spectrum in damaged sample.

In short, the nonlinearity due to the presence of the cracks is an extremely sensitive indicator of the presence of damage and a tool to monitor progressive damage. The undamaged portion of the sample produces a very small nonlinear response that is atomic in nature. The damaged portion of the material acts as a localized nonlinear mixer producing a significant, nonclassical nonlinear response (in contrast to a rock where the nonlinear response is volumetric). This behaviour is manifest in two primary ways when sound is applied to the object. Just as in volumetrically damaged granular materials, the effects of resonance frequency shift and generation of new frequency components can be large in damaged material but nearly unmeasurable in undamaged materials.

Figure 29a illustrates a method that exploits sideband mixing, which we term Nonlinear Wave Modulation Spectroscopy (NWMS) [89, 90]. In this method, an object is struck

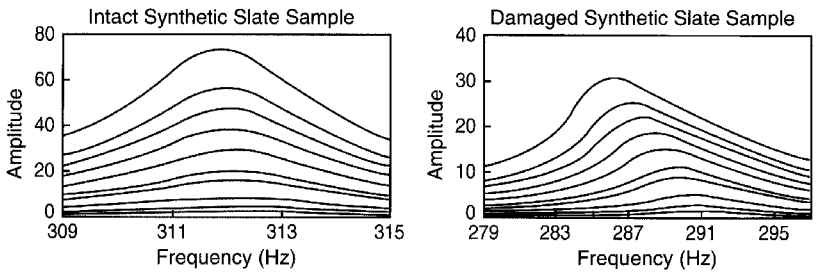

Fig. 30. – Nonlinear Resonant Ultrasound Spectroscopy (NRUS). Resonance curves at 10 different drive levels in undamaged (left), and damaged samples (right). The samples are rectangular strips of an artificial slate of 200 mm ×20 mm ×4 mm. The strips are excited at their lowest-order bending resonance mode (the resonance frequency is typically about 300 Hz).

by an impulse while being simultaneously driven by a pure-tone continuous wave. The impulse causes the sample to ring at its resonance modes, and those modes mix with the pure tone producing sidebands around the pure tone. We show spectra from experiments in undamaged and damaged automobile engine bearing caps in figs. 29b,c near the pure tone frequency of 115 kHz. The difference is impressive. The sample contains a crack several millimeters deep and about a centimeter long.

The resonance experimental procedure shown in fig. 4 and the result shown in fig. 5b can be employed to discern damage as well. Figure 30 illustrates results from this technique, termed Nonlinear Resonance Ultrasound Spectroscopy (NRUS), in samples of undamaged and damaged concrete-based slate reinforced with fiber, from Van Den Abeele *et al.* [91]. Clearly, the damaged sample is significantly more nonlinear (resonance curves more asymmetric) than the undamaged sample.

In all such experiments, it has been observed that the dependences with strain amplitude are the same as those observed in other highly nonlinear materials (*e.g.*, [25]).

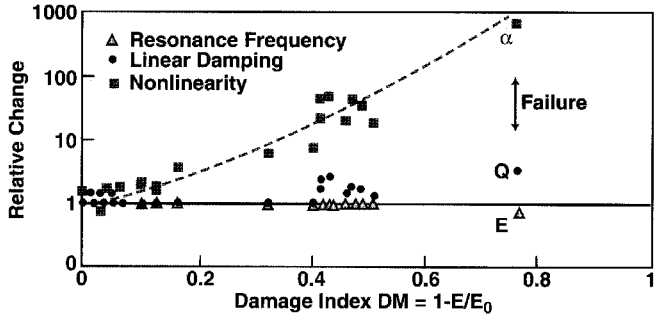

Fig. 31. – Change in normalized linear (resonance frequency and linear damping) and nonlinear response as a function of progressive damage. Each value is normalized to its linear value (the value at the beginning of the experiment before any damage has been induced). See text for more.

Progressive damage. The result of applying NRUS in a cyclic fatigue loading experiment in a large bar of concrete from [90] is shown in fig. 31. In the figure, the variation of the linear (resonance frequency and attenuation) and nonlinear (from resonance shift) material parameters with respect to their initial values as a function of the damage index DM are shown. In the experiment, the applied load was cycled up to 28 times, which is large enough to induce permanent fatigue damage after several hundreds of cycles. After each cycle during the test, the apparent instantaneous modulus, E, is calculated from quasi-static force-displacement curves. This value is then compared to the initial modulus value, E_0, and used to define a damage index DM, such that $DM = 1 - E/E_0$. It is clear that the nonlinear response is far more sensitive than the linear response in detecting the onset and progression of damage.

In summary, the above nonlinear methods illustrate the new frontier in acoustical nondestructive testing of materials for damage. In fact, measurement of nonlinear behaviour may well be the most sensitive method available for study and early detection and the progression of damage. There are potentially a huge number of applications of enormous economic and safety impact that will evolve from nonlinear applications. Several companies have already begun to develop sophisticated instruments for this type of analysis.

8. – Conclusions

From the experimental results outlined in this paper we infer that the micro-to-nanoscale "bond system" (microcracks, dislocations, etc.) is responsible for strong hysteretic nonlinearity. The bond system, which is a small fraction of the total volume of the material, links hard grains or crystals at scales of microns to millimeters, that are atomic elastic in nature and therefore contribute little to the elastic nonlinearity of the material. It is clear that this is an extremely rich area of material physics, one that bridges macroscopic behaviour, mesoscopic granular structure, and nanoscale features. A joint mechanical, thermodynamical and possibly even quantum-physics approach may be necessary for understanding the physics of nonlinearity in rocks. In addition, new problems in nonlinear wave theory must be addressed such as wave propagation and interaction in hysteretic media. At any rate, the fundamental and persistent problem of a full understanding of the mechanisms of strong nonlinearity in rocks and other similar materials remains to be solved, and this issue is currently being actively addressed.

* * *

This work was supported by the Office of Basic Energy Science of the United States Department of Energy under contracts W-7405-ENG-36 (Los Alamos National Laboratory) with the University of California; by the Institute of Geophysics and Planetary Physics at Los Alamos; by Defense Programs at Los Alamos; by Institutional Support at Los Alamos (LDRD); by the Russian Foundation for Basic Research; and by the NOAA Environmental Technology Laboratory. We thank R. Guyer, A. Sutin, V. Nazarov, A. Matveev, A. Potapov, I. Soustova, V. Zaitsev, I. Belyaeva, A. Korotkov, B. Zinszner, T. Shankland, B. Bonner, A. Migliori, F. Cohen-Tenoudji, J.-C. Lacoutur, I. Beresnev, K. Van Den Abeele, T. McEvilly, J. Ten Cate, K. McCall, P. Rasolofosaon, A. Zarembowich, P.-P. Delsanto, M. Scalerandi, V. Agnostini, T. Darling, J. Carmeliet, and many others for close collaboration in the work that led to this paper.

REFERENCES

[1] GUYER R. and JOHNSON P., *Phys. Today*, **52** (1999) 30.
[2] JOHNSON P., *Dynamic Elastic Nonlinearity in Earth Materials*, Doctoral Dissertation, University of Paris VI (1997), p. 103.
[3] VON WINKLE W., in *Scientific and Engineering Studies: Nonlinear Acoustics 1954 to 1983* (Naval Underwater Systems Center, Dept. of the US Navy, Newport Lab., Newport, RI) 1983; NOVIKOV B., RUDENKO O. and TIMOSHENKO V., *Nonlinear Underwater Acoustics* (AIP Press, Acoust. Soc. Amer., New York) 1987.
[4] ZAREMBO L. and KRASIL'NIKOV V., *Introduction to Nonlinear Acoustics* (Nauka, Moscow) 1966.
[5] GRANATO A. and LÜCKE K., *Appl. J. Phys.*, **27** (1956) 583.
[6] OSTROVSKY L., SOUSTOVA I. and SUTIN A., *Acustica*, **5** (1978) 298.
[7] NAUGOLNYKH K. A. and OSTROVSKY L. A., *Nonlinear Wave Processes in Acoustics* (Cambridge University Press, Cambridge-New York) 1998.
[8] BLACKSTOCK D. and HAMILTON M. (Editors), *Nonlinear Acoustics* (Academic Press, London-San Diego) 1998.
[9] BIRCH F., in *Handbook of Physical Constants*, edited by CLARK S. P. jr. (Geol. Soc. Am. Press, Connecticut) 1966, pp. 97-174.
[10] MCKAVANAGH B. and STACY F., *Phys. Earth Planet. Int.*, **8** (1974) 246.
[11] WINKLER K., NUR A. and GLADWIN M., *Nature*, **277** (1979) 528.
[12] BAKULIN V. and PROTOSENYA A., *Transactions (Doklady) of the USSR Academy of Sciences, Earth Sciences Sections*, **263** (1982) 314 (English translation: Scripta Publishing 1984).
[13] MCCALL K. and GUYER R., *Nonlin. Proc. Geophys.*, **3** (1996) 89.
[14] GUYER R., MCCALL K., BOITNOTT G., HILBERT L. and PLONA T., *J. Geophys. Res.*, **102** (1997) 5281.
[15] HILBERT L., HWONG T., COOK N., NIHEI K. and MYER L., in *Rock Mechanics Models and Measurements Challenges from Industry*, edited by NELSON P. P. and LAUBACH S. E. (Balkema A. A., Rotterdam) 1994, p. 497.
[16] JAEGER J. and COOK N., in *Fundamentals of Rock Mechanics*, 3rd edition (Chapman and Hall, London) 1979, p. 78.
[17] TUTUNCU A., PODIO A., GREGORY R. and SHARMA M., *Geophysics*, **63** (1998) 184.
[18] GIST G., *J. Acoust Soc. Am.*, **23** (1994) 1158.
[19] JOHNSON P., ZINSZNER B. and RASOLOFOSAON P., *J. Geophys. Res. B*, **101** (1996) .
[20] GUYER R., JOHNSON P. and TENCATE J., *Phys. Rev. Lett.*, **82** (1999) 3280.
[21] NAZAROV V., OSTROVSKY L., SOUSTOVA I. and SUTIN A., *Phys. Earth Planet Int.*, **50** (1988) 65.
[22] VAN DEN ABEELE K., CARMELIET J., JOHNSON P. and ZINSZNER B., to be published in *J. Geophys. Res.*
[23] TENCATE J. and SHANKLAND T., *Geophys. Res. Lett.*, **23** (1996) 3019.
[24] TENCATE J., SMITH J. and GUYER R., *Phys. Rev. Lett.*, **85** (2000) 1020.
[25] JOHNSON P., SUTIN A. and DARLING T., to be published in *Science*.
[26] BONNER B. and WANAMAKER B., in *Review of Progress in Quantitative NDE*, edited by THOMPSON D. and CHIMENTI D. B., Vol. **9B** (Plenum Press, New York and London) 1990, pp. 1709-1712; Vol. **10B**, 1991, pp. 1861-1867.
[27] JOHNSON P. and RASOLOFOSAON P., *Nonlin. Proc. Geophys.*, **3** (1996) 77.
[28] ISHIHARA K., *Soil Behaviour in Earthquake Geotechnics* (Clarendon Press, Oxford) 1996.
[29] NAZAROV V., OSTROVSKY L., SOUSTOVA I. and SUTIN A., *Acoust. Phys.*, **30** (1994) 827.
[30] PREISACH F., *Phys. Z.*, **94** (1935) 277; MAYERGOSZ J., *Appl. J. Phys.*, **57** (1985) 3803.
[31] HOLCOMB D., *J. Geophys. Res.*, **86** (1981) 6235.
[32] ZIMENKOV S. V. and NAZAROV V., *Izv. Earth Phys.*, **29** (1994) 12.
[33] MEEGAN G., JOHNSON P., GUYER R. and MCCALL K., *J. Acoust. Soc. Am.*, **94** (1993) 3387.
[34] JOHNSON P., HOPSON T. and SHANKLAND T., *J. Acoust. Soc. Am.*, **92** (1992) 2842.

[35] ZAITSEV V., KOLPAKOV A. and NAZAROV V., *Acoust. Phys.*, **45** (1999) 202, 305.
[36] JOHNSON P. and MCCALL K., *Geophys. Res. Lett.*, **21** (1994) 165.
[37] PESTORIUS F. and BLACKSTOCK D., in *Finite-Amplitude Wave Effects in Fluids, 1973 ISNA Symposium-Copenhagen*, edited by L. BJORNO (Techn. Univ. of Denmark) 1973, pp. 24-29.
[38] ROLLINS F., TAYLOR L. and TODD B., *Phys. Rev. A*, **136** (1964) 597; JONES G. and KOBETT D., *J. Acoust. Soc. Am.*, **35** (1963) 5.
[39] JOHNSON P., SHANKLAND T. O'CONNELL R. and ALBRIGHT J., *J. Geophys. Res.*, **92** (1987) 3597.
[40] JOHNSON P. and SHANKLAND T., *J. Geophys. Res.*, **94** (1989) 17729.
[41] LANDAU L. and LIFSHITS E., *Theory of Elasticity*, 3rd edition (Pergamon Press, Oxford) 1986.
[42] ZAREMBO L. and KRASIL'NIKOV V., *Sov. Phys. Usp.*, **13** (1971) 778.
[43] ASANO S., *J. Phys. Soc. Jpn.*, **29** (1970) 952.
[44] GUYER R., MCCALL K., JOHNSON P., RASOLOFOSAON P. and ZINSZNER B., in *1995 International Symposium on Rock Mechanics*, edited by DAEMON and SHULTZ (Balkema, Rotterdam) 1985, pp. 177-181.
[45] GUYER R., MCCALL K. and BOITNOTT G., *Phys. Rev. Lett.*, **74** (1995) 3491.
[46] BELYAEVA I., OSTROVSKY L. and TIMANIN E., *Acoust. Lett.*, **15** (1992) 221.
[47] BELYAEVA I., ZAITSEV V. and OSTROVSKY L., *Acoust. Phys.*, **39** (1993) 11; BELYAEVA I., OSTROVSKY L. and ZAITSEV V., *Nonlin. Proc. Geophys.*, **4** (1997) 1.
[48] BELYAEVA I., ZAITSEV V. and TIMANIN E., *Acoust. Phys.*, **40** (1994) 789.
[49] OSTROVSKY L., JOHNSON P. and SHANKLAND T., in *Nonlinear Acoustics at the Turn of the Millenium, ISNA 15, Göttingen, 1999*, edited by LAUTERBORN W. and KURZ T., (AIP, Melville, N.Y.) 2000, pp. 75-84.
[50] DERESEWICZ H., *Appl. Mech. Rev.*, **11** (1958) 259.
[51] BELYAEVA I. and ZAITSEV V., Preprint No. 405, Institute of Applied Physics, Nizhny Novgorod, 1996.
[52] YEKIMOV A., LEBEDEV A., OSTROVSKY L. and SUTIN A., *Acoust. Phys.*, **42** (1996) 51.
[53] WALSH J., *J. Geophys. Res.*, **70** (1965) 381.
[54] NAZAROV V. and SUTIN A., *Acoust. Phys.*, **41** (1995) 827.
[55] ZAITSEV V., SUTIN A., BELYAEVA I. and NAZAROV V., *Vibr. J. Control*, **1** (1995) 335.
[56] CLARK V. and TITTMAN B., *J. Geophys. Res. B*, **85** (1980) 5190; TITTMAN B., CLARK V. and RICHARDSON J., *J. Geophys. Res. B*, **85** (1980) 5199.
[57] BOURBIE T., COUSSY O. and ZINSZNER B., *Acoustics of Porous Media* (French Petrol. Inst., 27, Paris, Edition Technic.) 1986.
[58] TUTUNCU A. and SHARMA M., *Geophysics*, **57** (1992) 1571.
[59] NAZAROV V., *Acoust. Phys.*, **45** (1999) 92.
[60] ISRAELASHVILI J., *Intermolecular and Surface Forces, With Applications to Colloidal and Biological Systems* (Academic Press, Boston) 1985.
[61] CARMELIET J., HOUVENAGHEL G. and DESHAMPS F., *Transport in Porous Materials*, **35** (1999) 67.
[62] NORRIS A. and JOHNSON D., *Appl. J. Mech.*, **64** (1997) 39; JOHNSON D., ELATA D., BERRYMAN J., HORNBY B. and NORRIS A., *Trans. ASME*, **65** (1998) 380; JOHNSON D., MAKSE H., GLAND N. and SCHWARTZ L., *Physica B*, **279** (2000) 134.
[63] BONNER B., BERGE P., ARACHNE-RUDDLE C., BORO C., HARDY E. and TROMBINO C., in *Proceedings of the Symposium on the Application of Geophysics to Engineering and Environmental Problems (SAGEEP), Oakland, CA*, edited by CRAMER L. and BELL R. (Environm. and Eng. Geophys. Soc., Wheat Ridge, CO) 1999, pp. 455-463.
[64] GUYER R., MCCALL K. and VAN DEN ABEELE K., *Geophys. Res. Lett.*, **25** (1998) 1585.
[65] VAN DEN ABEELE K., *J. Acoust. Soc. Am.*, **99** (1996) 3334; VAN DEN ABEELE K. and JOHNSON P., *J. Acoust. Soc. Am.*, **99** (1996) 3346.
[66] JOSSERAND C., TKACHENKO A., MUETH D. and JAEGER H., *Phys. Rev. Lett.*, **85** (2000) 3632.
[67] NAZAROV V. and SUTIN A., *Sov. Phys. Acoust.*, **35** (1989) 410.

[68] NAZAROV V., *Acoust. Phys.*, **43** (1997) 192.
[69] VAN DEN ABEELE K., JOHNSON P., GUYER R. and MCCALL K., *J. Acoust. Soc. Am.*, **101** (1997) 1885.
[70] GUSEV V., GLORIEUX C., LAURIKS J. and THOEN W., *Phys. Lett. A*, **232** (1997) 77.
[71] GUSEV V., BAILLIET H., LOTTON P. and BRUNEAU M., *Wave Motion*, **29** (1999) 211.
[72] NAZAROV V., OSTROVSKY L., SOUSTOVA I. and RADOSTIN A., in *Nonlinear Acoustics at the Turn of the Millenium, ISNA 15, Göttingen, 1999*, edited by LAUTERBORN W. and KURZ T. (AIP, Melville, N.Y.) 2000, pp. 299-302.
[73] VAN DEN ABEELE K. and TENCATE J., to be published in *J. Geophys. Res.*
[74] DAY S. and MINSTER J., *Geophys. J. R. Astr. Soc.*, **78** (1984) 105.
[75] DELSANTO P., WHITCOMBE H., CHASKELIS H. and MIGNIGNA R., *Wave Motion*, **15** (1992) 65; **20** (1994) 297; **26** (1997) 329.
[76] BERESNEV I. and NIKOLAEV A., *Phys. Earth Planet Int.*, **50** (1988) 83.
[77] NIKOLAEV A., PAVLENKO O. and YAKOVLEV A., *Phys. Solid Earth*, **30** (1995) 1023.
[78] BAGMET A., NAZAROV V. and NIKOLAEV A., *Phys. Solid Earth*, **31** (1996) 622.
[79] AGNEW D., *J. Geophys. Res.*, **86** (1981) 3969.
[80] BEAVAN J. and GOULTY N., *Geophys. J. R. Astron. Soc.*, **48** (1977) 293.
[81] ZINSZNER B., JOHNSON P. and RASOLOFOSAON P., *J. Geophys. Res.*, **102** (1997) 8105.
[82] MAY J., *IRE Natl. Conv. Rec.*, **6** (1958) 134.
[83] SHEARER P. and ORCUTT J., *Bull. Seism. Soc. Am.*, **77** (1987) 1168.
[84] BERESNEV I. and WEN K., *Bull. Seism. Soc. Am.*, **86** (1996) 1964.
[85] FIELD E., JOHNSON P., ZENG I. and BERESNEV I., *Nature*, (1997) 599; FIELD E., ZENG I., JOHNSON P. and BERESNEV I., *J. Geophys. Res.*, **103** (1998) 26869.
[86] KLUZEK Z., SUTIN A., MATVEEV A. and POTAPOV A., *Acoust. Lett.*, **18** (1995) 198.
[87] KOROTKOV A. and SUTIN A., *Acoust. Lett.*, **18** (1994) 59.
[88] VAN DEN ABEELE K. and DE VISSCHER J., *Cement and Concrete Research, AIP Conf. Proc.* (2000) 341.
[89] JOHNSON P., *Materials World, J. Inst. Materials*, **7** (1999) 544.
[90] VAN DEN ABEELE K., JOHNSON P. and SUTIN A., *Res. Nondestruc. Eval.*, **12** (2000) 17.
[91] VAN DEN ABEELE K., CARMELIET J., TENCATE J. and JOHNSON P., *Res. Nondestruc. Eval.*, **12** (2000) 31.
[92] ZHURKOV S., *Sov. Phys. Solid State*, **25** (1983) 1797; PETROV V., *Sov. Phys. Solid State*, **25** (1983) 1800.

LAST PUBLISHED PAPERS

L. LUCCHETTI and F. SIMONI - Soft materials for optical storage

A. BONASERA, M. BRUNO, C. O. DORSO and P. F. MASTINU - Critical phenomena in nuclear fragmentation

M. BARGIOTTI, A. BERTIN, M. BRUSCHI, M. CAPPONI, S. DE CASTRO, R. DONÀ, P. FACCIOLI, D. GALLI, B. GIACOBBE, U. MARCONI, I. MASSA, M. PICCININI, M. POLI, N. SEMPRINI CESARI, R. SPIGHI, V. VAGNONI, S. VECCHI, M. VILLA, A. VITALE and A. ZOCCOLI - Present knowledge of the Cabibbo-Kobayashi-Maskawa matrix

M. LABARDI, P. G. GUCCIARDI and M. ALLEGRINI - Near-field optical microscopy

MICHELE MODUGNO - Thermodynamics of the Gross-Neveu model beyond the mean-field approximation

G. CHIRICO and C. GROPPI - Applications of fluctuation spectroscopy to biomolecules

R. CESAREO - X-ray physics: Interaction with matter, production, detection

M. MILANI, M. COSTATO, F. BRIVIO, R. CASATI, G. CATTANEO, F. MAGNI, N. C. PISTONI, F. PREVIDI and L. SPINOGLIO - A critical analysis of radiation-matter interaction

N. LO IUDICE - Collective excitations in deformed nuclei

GIORGIO SEDMAK - Wide-field optical technologies in astronomy

A. D. POLOSA - The CQM model

A. EREDITATO and P. MIGLIOZZI - Accelerator studies of neutrino oscillations

GRZEGORZ P. KARWASZ, ROBERTO S. BRUSA and ANTONIO ZECCA - One century of experiments on electron-atom and molecule scattering: a critical review of integral cross-sections II. – Polyatomic molecules

M. BEZZI - Modeling evolution and immune system by cellular automata

ROBERTO LUZZI, ÁUREA R. VASCONCELLOS and J. GALVÃO RAMOS - Irreversible thermodynamics in a nonequilibrium statistical ensemble formalism

GRZEGORZ P. KARWASZ, ROBERTO S. BRUSA and ANTONIO ZECCA - One century of experiments on electron-atom and molecule scattering: A critical review of integral cross-sections III. – Hydrocarbons and halides

C. FAVUZZI, N. GIGLIETTO, M. N. MAZZIOTTA and P. SPINELLI - Transition radiation detectors for particle physics and astrophysics

FORTHCOMING PAPERS (in alphabetical order)

S. ALESSIO and A. LONGHETTO - The detection of travelling disturbances in meteo-climatic fields

P. CALVANI - Optical properties of polarons

P. SHIKTOROV, E. STARIKOV, V. GRŭZINSKIS, T. GONZÁLEZ, J. MATEOS, D. PARDO, L. REGGIANI, L. VARANI and J. C. VAISSIÈRE - Transfer-field methods for electronic noise in submicron semiconductor structures